

X-640-64-383

NASA TMX-55163

FACILITY FORM 502

N65-18276

(ACCESSION NUMBER)

58

(PAGES)

TMX-55163

(NASA CR OR TMX OR AD NUMBER)

(THRU)

(CODE)

13

(CATEGORY)

# PROPAGATION OF THE PRESSURE WAVES PRODUCED BY AURORAS

BY

KAICHI MAEDA

GPO PRICE \$

OTS PRICE(S) \$

Hard copy (HC)

Microfiche (MF)

\$3.00

\$0.50

DECEMBER 1964

NASA

GODDARD SPACE FLIGHT CENTER

GREENBELT, MD.

Presented at the Second Benedum Earth Symposium  
Pittsburgh, Pennsylvania  
November 23-25, 1964

X-640-64-383

PROPAGATION OF THE PRESSURE WAVES

PRODUCED BY AURORAS

Kaichi Maeda  
Goddard Space Flight Center  
Greenbelt, Maryland

Goddard Space Flight Center  
Greenbelt, Maryland

Presented at the Second Benedum Earth Symposium,  
Pittsburgh, Pennsylvania, November 23-25, 1964

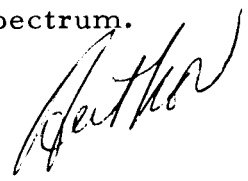
## CONTENTS

	Page
Abstract . . . . .	ii
1. Introduction . . . . .	1
2. Equations of Atmospheric Pressure Waves . . . . .	2
2.1 Notations and Constants . . . . .	2
2.2 Fundamental Equations . . . . .	4
3. Solutions in the Isothermal Atmosphere . . . . .	6
3.1 Diagnostics . . . . .	7
3.2 Dispersions . . . . .	9
4. Solutions in the Non-Isothermal Atmosphere . . . . .	10
4.1 Diagnostics . . . . .	15
4.2 Dispersions . . . . .	18
5. Normal Mode Calculation . . . . .	19
5.1 Multi-Isothermal Layer Model . . . . .	20
5.2 W.K.B. - Approximation . . . . .	30
5.3 Direct Numerical Integration . . . . .	34
6. Data Analysis . . . . .	36
6.1 Power Spectrum Analysis . . . . .	39
6.2 Wave Form and Airy Phase . . . . .	46
7. Discussion . . . . .	47

## Abstract

18276

As shown in previous paper (Maeda and Watanabe), periodic heating around E-region in the polar upper atmosphere by auroral particles can be regarded as the source of very long acoustic type atmospheric pressure waves observable at the ground. It was shown, however, that these pressure waves attenuate rapidly outside the source in the isothermal atmosphere. On the other hand, in the actual atmosphere, these waves propagate horizontally through the ducting, which consists of two channels, corresponding to the atmospheric temperature minima at the mesopause and the tropopause, respectively. It is shown that for the propagation of 100 sec waves, upper channel is effective in summertime, while lower one is effective in winter in the polar upper atmosphere. It is also shown that the traveling pressure waves associated with auroral activity is not necessarily limited in the acoustic mode, but sometimes extended to gravity (thermobaric) mode. This is partly due to the existence of large positive lapse rates layers such as upper part of stratosphere and in the thermosphere. As a consequence, clear sinusoidal oscillations, which appear occasionally with periods of group velocity minima (around 5 min), can be ascribed to Airy phase. As an example, the data obtained at the NBS-stations in Washington, D.C. on July 15, 1960 are shown with its preliminary results of power spectrum.



# PROPAGATION OF THE PRESSURE WAVES PRODUCED BY AURORAS

## 1. Introduction

During intervals of high geomagnetic activity, trains of long period acoustic waves have been detected at the ground (Chrzanowski et. al. 1961). Investigating these phenomena, we found that these travelling pressure waves must be originated by auroral activities and that one of the most plausible generation mechanisms of these atmospheric pressure waves is periodic heating of E-region in the polar upper atmosphere caused by imping auroral electrons (Maeda & Watanabe,\* 1964a, b).

Correspondences between auroral activities and appearances of infrasonic waves are further confirmed by the special observation performed inside of auroral zone (Campbell and Young, 1963). Assuming a certain distribution of auroral heating, which is very similar to the observed auroral luminosity distribution, we could show relations between input thermal energy, which can be assumed as some fractions of incident energy flux of auroral electrons, and intensity of acoustic wave at the ground, with respect to the isothermal atmosphere. We found, however, that the intensities of these long period pressure waves produced by auroral heating of polar upper air attenuate very rapidly outside of the source region.

---

\*In late, this paper will be referred as M-W, 1.

Although the auroral activities are spread toward low latitudes at the time when these pressure waves are detected at the ground, horizontal propagations of these waves in the atmosphere outside of the source region are important to explain the diurnal variation of arrival direction of the wave observed at NBS-stations in Washington, D.C.

Since previous calculations were based on an isothermal atmosphere, contribution of atmospheric thermal structure on the wave-propagation was not considered.

It is, therefore, a main purpose of this paper to discuss the effect of atmospheric thermal structure on the propagations of auroral infrasonic waves.

The traveling pressure waves which appear at the time of strong auroral activities are quite different from well-known long period pressure waves produced by other phenomena such as large meteor, volcano eruption or huge bomb explosion in the atmosphere. Due to the dispersive character of atmospheric wave, intensity, duration, forms and their time variation of these waves are complicated. However, some peculiar features can be explained by the known dispersion relations. This will be discussed in the last chapter.

## 2. Equations of Atmospheric Pressure Waves

### 2.1 Notations and Constants

$c$ , sound velocity in the air in km/sec

$D/Dt$ , the Eulerian derivative,  $\frac{\partial}{\partial t} + \nabla \cdot \mathbf{V}$

- $g(0, -g)$ , acceleration of gravity where  $g = 9.8 \cdot 10^{-3}$  km/sec.<sup>2</sup>
- $H$ , scale height in km.
- $f$ , resultant of all external forces.
- $k$ , horizontal wave number, corresponding to horizontal wave length  $\lambda$  (in km), i.e.  $k = 2\pi/\lambda$  in km<sup>-1</sup>.
- $p, \rho, T$ ; small departure from static value of pressure, density and temperature function of time ( $t$ ) and altitude ( $z$ ).
- $p_0, \rho_0, T_0$ , static pressure, density and absolute temperature, which are the function of altitude  $z$ , only, in dynes/cm<sup>2</sup>, g/cm<sup>3</sup> and °K, respectively.
- $\bar{p}, \bar{\rho}, \bar{T}$ , total pressure, density and absolute temperature, i.e.  

$$\bar{p} = p_0 + p, \bar{\rho} = \rho_0 + \rho, \bar{T} = T_0 + T$$
- $R$ , gas constant of air,  $2.87 \cdot 10^{-4}$  in km<sup>2</sup> sec<sup>-2</sup> °K<sup>-1</sup>.
- $\bar{V} = \bar{V}(u, w)$ ; velocity vector, where  $u$  is horizontal (southward), and  $w$  is vertical (upward) component of air motion in km/sec.
- $\gamma$ , ratio of specific heat of air,  $C_p/C_v$ , where  $C_p$  and  $C_v$  are the specific heat of air at constant pressure and that at constant volumen, respectively.
- $\lambda$ , horizontal wave length of pressure wave is km.
- $\tau$ , period of pressure wave in sec.
- $\chi(\omega, z)$ , the divergence of velocity in sec<sup>-1</sup>. i.e.  $\chi = \partial u / \partial x + \partial w / \partial z$
- $\omega$ , angular frequency of pressure wave corresponding to period of wave  $\tau$  (sec) in sec<sup>-1</sup>.

## 2.2 Fundamental Equations

Equation of atmospheric waves is derived from the following three fundamental equations; namely the equation of motion

$$\frac{D\bar{V}}{Dt} + \frac{1}{\bar{\rho}} \nabla \cdot \bar{p} = f \quad (2.1)$$

the equation of continuity

$$\frac{D}{Dt} \left( \frac{1}{\bar{\rho}} \right) = - \frac{1}{\bar{\rho}} \nabla \cdot \bar{V} \quad (2.2)$$

and the equation of thermodynamics

$$\frac{D\bar{p}}{Dt} = c^2 \frac{D\bar{\rho}}{Dt} \quad (2.3)$$

Since the excitation of auroral infrasonic waves occurs mainly along auroral zone, which is extended in a certain latitude, the propagation of the wave along meridian toward low latitudes can be treated in two dimensions, taking horizontal axis  $x$  southward and vertical axis  $z$  upward.

Period of wave in our present subject is less than several ten minutes, therefore, the Coriolis force due to the earth's rotation and all other external forces except gravity, can be neglected. The equation of motion (2.1) then becomes

$$\rho_0 \frac{\partial u}{\partial t} = - \frac{\partial p}{\partial t} \quad (2.4)$$

and

$$\rho_0 \frac{\partial w}{\partial t} = - \frac{\partial p}{\partial z} - g \rho$$

The equation of continuity (2.2) for the first order approximation is

$$\frac{\partial \rho}{\partial t} + \mathbf{W} \cdot \frac{\partial \rho_0}{\partial \mathbf{z}} = -\rho_0 \cdot \chi \quad (2.5)$$

where  $\chi = \chi(\mathbf{p}, \mathbf{z}, t)$  is the velocity divergence.

By making use of Eq. (2.5), the equation of thermodynamics (2.3) can be written as

$$\frac{\partial \mathbf{p}}{\partial t} + (c^2 \chi - \mathbf{W} \cdot \mathbf{g}) \rho_0 = 0 \quad (2.6)$$

Assuming that  $u, w, p$  and  $\rho$  are proportional to a factor  $e^{i(\omega t - k z)}$  we get an equation for the vertical variation of  $\chi(\omega, z)$ .

$$\frac{d^2 \chi}{dz^2} - 2N(z) \frac{d\chi}{dz} + M^2(z) \chi = 0 \quad (2.8)$$

where

$$N(z) = \frac{1}{2H(z)} \left[ 1 - \frac{dH(z)}{dz} \right] \quad (2.9)$$

$$M^2(z) = \frac{\omega^2}{c^2(z)} - k^2 \left[ 1 - \frac{\omega_B^2}{\omega^2} \right] \quad (2.10)$$

$$c^2(z) = \gamma g H(z), \quad H(z) = RT(z)/g \quad (2.11)$$

and

$$\omega_B^2 = \frac{g^2}{c^2} (\gamma - 1) + \frac{g}{c^2} \frac{dc^2}{dz} \quad (2.12)$$

$\omega_B$  is called Brunt angular frequency or Vaisala angular frequency.

This can also be written as

$$\omega_B^2 = g \frac{d \ln \Theta}{dz} \quad (2.13)$$

where  $\Theta$  is potential temperature (Gossard, 1962).

### 3. Solutions in the Isothermal Atmosphere

In the case of isothermal atmosphere,  $dH/dz = 0$  and  $N, M^2$  in Eq. (2.8) are constant. Then as discussed in M-W, 1 the solution of (2.8) is given by M - W, 1.

$$\chi(\omega, z) = e^{Nz} (Ae^{-\mu z} + Be^{\mu z}) \quad (3.1)$$

where A and B are constants which should be determined by boundary conditions.

$$N = \frac{1}{2H} = \frac{\gamma g}{2c^2} \quad (3.2)$$

or

$$N = \frac{\omega_A}{c}, \quad \omega_A = \frac{\gamma g}{2c} \quad (3.3)$$

$\omega_A$  is called atmospheric acoustic resonance angular frequency or can be named Hines' angular frequency for a simplicity (Hines, 1964).

The solution (3.1) is oscillatory or exponential function of  $z$ , if  $\mu^2 = N^2 - M^2$  is negative or positive, respectively. Namely, if

$$N^2 - M^2 = \frac{\omega_A^2 - \omega^2}{c^2} + k^2 \left( 1 - \frac{\omega_b^2}{\omega^2} \right) > 0 \quad (3.4)$$

where

$$\omega_b^2 = \frac{g^2}{c^2} (\gamma - 1) \quad (3.5)$$

( $\omega_b$  is Brunt-Vaisala Angular frequency in the isothermal atmosphere.)

Then  $\mu$  is real and solution (3.1) corresponds to external (or exponential) solution, which is called non-cellular solution previously

(M-W,1, Maeda, 1964) strictly speaking, cellular wave is standing wave as named by Martyn (1950) and has been used by many workers (Yamanoto; 1956, Gossard, 1962). It would be therefore, better to avoid this nomenclature unless we consider the same case of cellular and non-cellular waves in the atmosphere, as discussed by Martyn (Hines, 1964). If  $N^2 - M^2 < 0$ , then it can be written that  $\mu = i\eta$ , where

$$\eta^2 = M^2 - N^2 = \frac{\omega^2 - \omega_A^2}{c^2} - k^2 \left( \frac{\omega^2 - \omega_b^2}{\omega^2} \right) > 0 \quad (3.6)$$

is the wave number in vertical direction. The solution (3.1) is written in this case

$$X(\omega, z) = e^{Nz} (Ae^{-i\eta z} + Be^{i\eta z}) \quad (3.7)$$

This corresponds to internal (or sinusoidal) waves, which are also called cellular solutions (Yamanoto, 1956, Gossard 1962, M-W,1, Maeda 1964). Due to the reason mentioned above, this nomenclature should be avoided unless it is used in the same sense as defined by Martyn (1950).

### 3.1 Diagnostics.

Since  $k$  is the wave number in horizontal direction, while  $\eta$  is the one in vertical direction as shown in (3.7), Eq. (3.6) gives the propagation surface (or propagation line in  $x - z$  cross-section). Namely, as discussed by several authors (Hines 1960, Eckart 1960, Tolstoy 1963 and M-W,1);

(i) if

$$\omega > \omega_A (> \omega_b)$$

propagation surface is ellipsoid with a major axis in x-direction, which half length  $k_c$  is given by

$$k_c = \frac{\omega}{c} \left( \frac{\omega^2 - \omega_A^2}{\omega^2 - \omega_b^2} \right)^{1/2} \quad (3.8)$$

and a minor axis in z-direction, which is also rotation axis of the ellipsoid and the half length  $\eta_c$  is

$$\eta_c = \frac{(\omega^2 - \omega_A^2)^{1/2}}{c} \quad (3.9)$$

(ii) if

$$\omega < \omega_b (< \omega_A),$$

propagation surface is hyperboloid with semi-major axis in x-direction, which is also given by (3.8) or

$$k_c = \frac{\omega}{c} \sqrt{\frac{\omega_A^2 - \omega^2}{\omega_b^2 - \omega^2}} \quad (3.8)$$

and this mode is called internal gravity, or thermobasic wave.

(iii) if

$$\omega_A > \omega > \omega_b$$

vertical wave number  $\eta$  defined by Eq. (3.6) is imaginary or  $\mu$  in Eq. (3.1) is real, indicating the wave motion in vertical direction is not oscillatory.

Although two types of waves within this frequency range in the isothermal atmosphere, which satisfy the boundary conditions at the ground and at infinity, are shown by Pekeris (1948 and see M-W,1), only one type called Lambs' wave (Lamb 1932, 1948) can exist in this frequency range (Hunt et al 1960). This wave propagates only in horizontal direction (Eckart 1960 p. 105).

### 3.2 Dispersions

As it can be seen from Eq. (3.6) vertical and horizontal wave numbers are functions of angular frequency, i.e., acoustic mode and internal gravity mode are both dispersive.

Phase velocity in horizontal direction is given from Eq. (3.6)

$$V_{ph} = \frac{\omega}{k} = c \sqrt{\frac{\omega^2 - \omega_b^2}{\omega^2 - \omega_A^2}} \quad \text{for acoustic mode} \quad (3.7)$$

From this equation we can see that at high frequency i.e. at  $\omega \rightarrow \infty$

$$V_{ph} = c$$

while as  $\omega \rightarrow \omega_A$

$$V_{ph} \rightarrow \infty.$$

Similarly for thermobasic mode, we can write from Eq. (3.6)

$$V_{ph} = c \sqrt{\frac{\omega_b^2 - \omega^2}{\omega_A^2 - \omega^2}}. \quad (3.8)$$

From this equation, we can see that at low frequency i.e. at  $\omega \rightarrow 0$

$$V_{ph} = c \cdot \frac{\omega_b}{\omega_A} \simeq 0.904 c$$

while as  $\omega \rightarrow \omega_b$

$$V_{ph} \rightarrow 0.$$

On the other hand, horizontal group velocities are given from Eq. (3.6) for acoustic mode

$$V_g = \frac{\omega}{k} = c \frac{(\omega^2 - \omega_A^2)^{1/2} (\omega^2 - \omega_b^2)^{3/2}}{\omega^4 - 2\omega^2 \omega_b^2 + \omega_A^2 \omega_b^2} \quad (3.9)$$

This shows that at high frequency i.e.  $\omega \rightarrow \infty$

$$V_g = c$$

while as  $\omega \rightarrow \omega_A$

$$V_g = 0$$

Similarly for thermobaric mode

$$V_g = c \frac{(\omega_A^2 - \omega^2)^{1/2} (\omega_b^2 - \omega^2)^{3/2}}{\omega_A^2 \omega_b^2 - 2\omega^2 \omega_b^2 + \omega^4} \quad (3.10)$$

and this gives at low frequency i.e.  $\omega \rightarrow 0$

$$V_g = c \cdot \frac{\omega_b}{\omega_A} = 0.904 c$$

while at  $\omega \rightarrow \omega_b$   $V_g = 0$ .

Summarizing above relation, we can see atmospheric acoustic wave approaches usual sound wave at high frequency of which phase and group velocity both approach round velocity  $c = \sqrt{\gamma kT}$ . On the other hand as  $\omega$  approaches to  $\omega_A$  phase velocity increases to infinity while group velocity tends to zero. At low frequency both phase and group velocity of thermobaric wave converge to

$$c \cdot 2\sqrt{\gamma - 1}/\gamma \simeq 0.904 c$$

while as  $\omega \rightarrow \omega_b$ , phase and group velocity approaches to zero.

These are shown in Fig. 1 for  $T = 300^\circ\text{K}$  isothermal atmosphere.

#### 4. Solutions in the Non-Isothermal Atmosphere

The second term in Eq. (2.8) can be eliminated by the following transform;

$$y = \int_0^z \frac{dz}{H(z)} \quad \text{or} \quad \frac{dy}{dz} = \frac{1}{H(z)} \quad (4.1)$$

and

$$\chi(z) = e^{\frac{y}{2}} \phi(y) \quad (4.2)$$

then Eq. (2.8) becomes

$$\frac{d^2\phi}{dy^2} + K^2(y) \cdot \phi(y) = 0 \quad (4.3)$$

where

$$K^2 = H^2 \cdot \eta^2 \quad (4.4)$$

and

$$\eta^2 = \frac{\omega^2 - \omega_A^2}{c^2} - k^2 \left[ 1 - \frac{\omega_B^2}{\omega^2} \right] \quad (4.5)$$

$\omega_A$  and  $\omega_B$  are the same as the one given by (3.3) and (2.12), respectively.

It should be noticed that  $\omega_A$  is a function of atmospheric temperature  $T(z)$  only, but  $\omega_B$  depends not only on  $T(z)$  but also on the temperature gradient  $dT/dz$  at each altitude  $z$ , as shown by Eq. (2.12). Since there

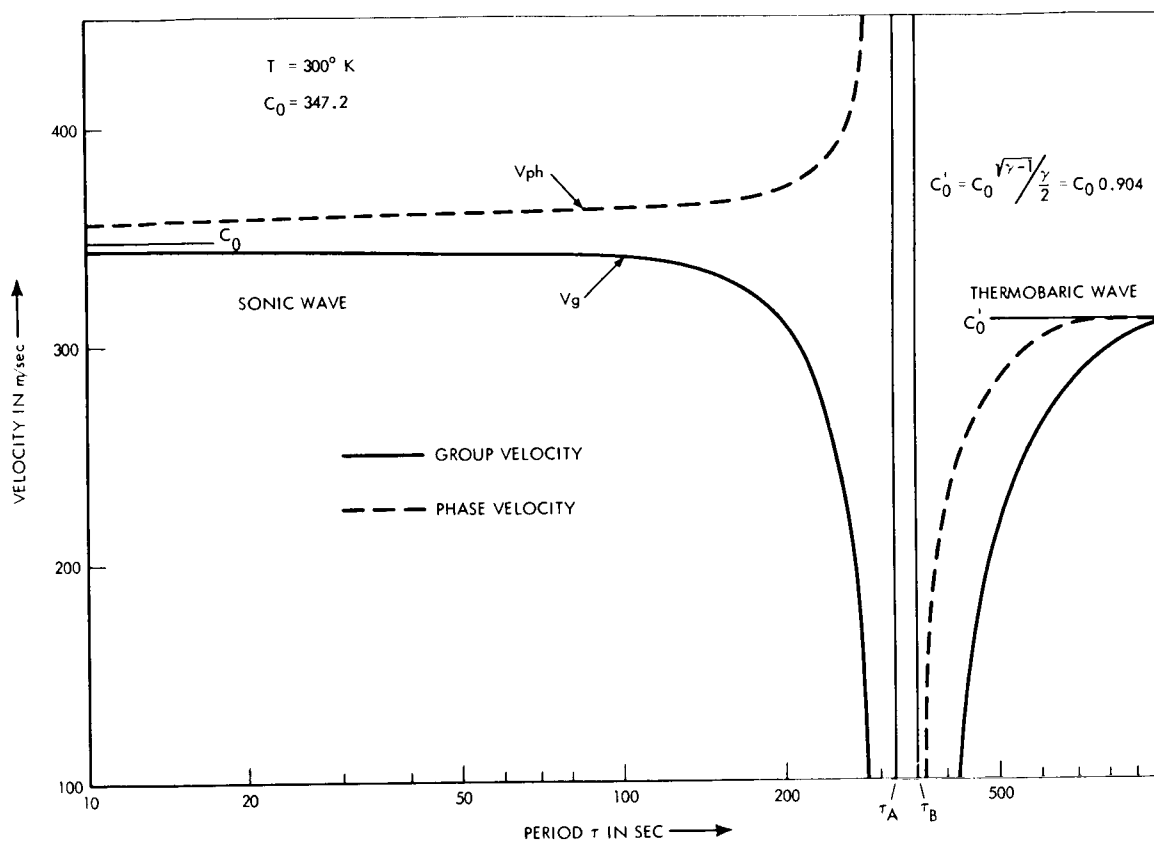


Figure 1—Horizontal wave velocities in the isothermal atmosphere ( $T = 300^\circ \text{K}$  and  $C = 0.347$  km/sec) against period of the wave  $\tau$  (in. sec) full lines and dashed lines are phase velocities and group velocities, respectively.

has been a confusion about the definition of  $\omega_A$  as pointed out by Hines (1964), it would be worthwhile to see the relation between  $\omega_A$  and  $\omega_B$ .

Rewriting the right hand side of Eq. (2.12), we get

$$\omega_B^2 = \left(\frac{\gamma g}{2c}\right)^2 - \left(\frac{g}{c} \cdot \frac{\gamma - 2}{2}\right)^2 + \frac{g}{c^2} \cdot \frac{dc^2}{dz}$$

Using Eq. (3.3), this becomes

$$\omega_A^2 = \omega_B^2 + \Delta\omega^2 \quad (4.6)^*$$

where

$$\begin{aligned} \Delta\omega^2 &= \frac{g^2}{c^2} \left(\frac{2 - \gamma}{2}\right)^2 - \frac{g}{c^2} \cdot \frac{dc^2}{dz} \\ &= \frac{g}{T(z)} \cdot \left[ \frac{g}{R} \left(\frac{2 - \gamma}{2}\right)^2 \cdot \frac{1}{\gamma} - \frac{dT(z)}{dz} \right] \end{aligned} \quad (4.7)$$

and

$$\frac{g}{R} = 34.2 \text{ } ^\circ\text{C/Km} \quad (4.8)^{**}$$

Therefore, if we write

$$\Gamma = \frac{g}{R} \left(\frac{2 - \gamma}{2}\right)^2 \cdot \frac{1}{\gamma} (\cong 2.2 \text{ } ^\circ\text{C/Km})$$

---

\*Eq. (4.6) might correspond to Eq. (4),  $N_1^2 = N^2 + \Gamma^2 c^2$  in Eckart's book (p. 108). However, as can be seen from (4.7),  $\Delta\omega^2$  is not necessarily positive, as  $\Gamma^2 c^2$  is.

\*\*Negative value of this value is called auto-convective lapse rate in meteorology.

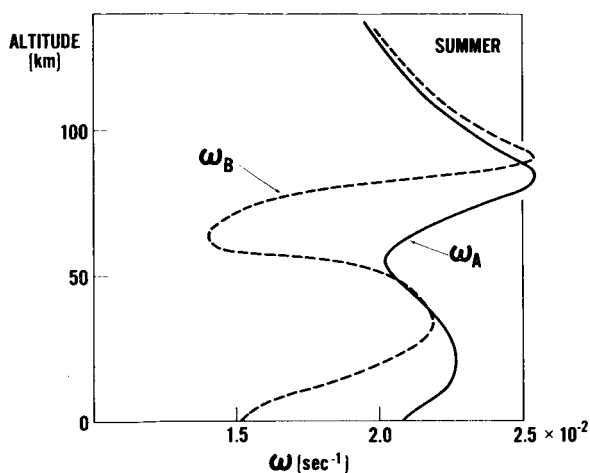


Figure 2—Hines' angular frequency  $\omega_A$  and Brunt-Varsola angular frequency  $\omega_B$  as a function of altitude  $z$ , for the vertical temperature distribution  $T(z)$  shown by full line in Fig. 4.

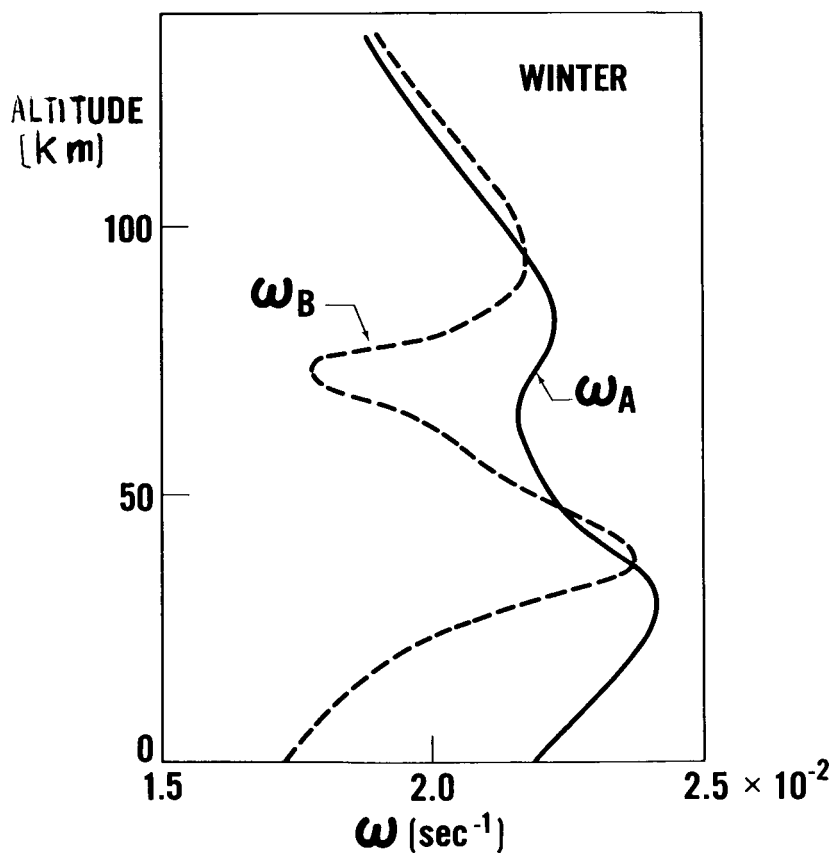


Figure 3—The same as Fig. 2 for the vertical temperature distribution shown in Fig. 4 by dashed line.

$$\Delta\omega^2 > 0 \ (\omega_A > \omega_B) \quad \text{if} \quad \frac{dT}{dz} < \Gamma_c$$

but

(4.9)

$$\Delta\omega^2 < 0 \ (\omega_A < \omega_B) \quad \text{if} \quad \frac{dT}{dz} > \Gamma_c$$

In Fig. 2 and Fig. 3  $\omega_A$  and  $\omega_B$  are shown as a function of altitude  $z$ , corresponding to mean polar atmosphere in summer and in winter, which temperature distributions are shown in Fig. 4 by full and dashed lines, respectively.

As can be seen from these figures, in the actual atmosphere there are in general two domains when  $\omega_B$  exceeds  $\omega_A$ , i.e., in the upper part of the stratosphere and in the thermosphere.

#### 4.1 Diagnostics

As far as  $\omega_B < \omega_A$ , diagnostics diagrams are essentially the same as in the isothermal atmosphere as discussed in M-W,1 (Eckart 1960 p. 108) and propagation surface for two modes (acoustic and internal gravity waves) are ellipsoid and hyperboloid, respectively (Eckart 1960, p. 110, Hines 1960, Obayashi 1963).

However, as shown in previous section (Fig. 2 & 3),  $\omega_B$  becomes larger than  $\omega_A$  in the upper stratosphere and in the thermosphere. In this domain propagation surfaces in  $y$ - $z$  space are as follows:

(i)  $\omega > \omega_B > \omega_A$

From Eq. (4.5), we can see propagation surface is ellipsoid, i.e.,

$$\frac{k^2}{k_c^2} + \frac{\eta^2}{\eta_c^2} = 1 \quad (4.10)$$

where

$$k_c^2 = \frac{\omega^2}{c^2} \cdot \frac{\omega^2 - \omega_A^2}{\omega^2 - \omega_B^2} \quad (4.11)$$

and

$$\eta_c^2 = \frac{\omega^2 - \omega_A^2}{c^2} \quad (4.12)$$

This corresponding acoustic mode discussed in (i), section 3.1.

(ii)  $\omega < \omega_A < \omega_B$

From Eq. (4.5) the propagation surface is hyperboloid

$$\frac{k^2}{k_c^2} - \frac{\eta^2}{\eta_c^2} = 1 \quad (4.13)$$

where

$$k_c^2 = \frac{\omega^2}{c^2} \cdot \frac{\omega_A^2 - \omega^2}{\omega_B^2 - \omega^2} \quad (4.14)$$

and

$$\eta_c^2 = \frac{\omega_A^2 - \omega^2}{c^2} \quad (4.15)$$

Propagation of this type of wave is limited in horizontal direction, corresponding to internal gravity (or thermobasic) waves discussed in (ii) section 3.1.

(iii)  $\omega_A < \omega < \omega_B$

The propagation surface is, then

$$\frac{\eta^2}{\eta_c^2} - \frac{k^2}{k_c^2} = 1 \quad (4.16)$$

where

$$\eta_c^2 = \frac{\omega^2 - \omega_A^2}{c^2} \quad (4.17)$$

and

$$k_c^2 = \frac{\omega^2}{c^2} \cdot \frac{\omega^2 - \omega_A^2}{\omega_B^2 - \omega^2} \quad (4.18)$$

As can be seen from (4.16), i.e.

$$|\eta| = \eta_c \cdot \sqrt{1 + \frac{k^2}{k_c^2}} > \eta_c > 0. \quad (4.19)$$

Namely, propagation of this type of wave is a hyperboloid limited in vertical direction with an asymptotic aperture

$$\theta_c = \text{tg}^{-1} \frac{k_c}{\eta_c} = \text{tg}^{-1} \left( \frac{\omega^2}{\omega_B^2 - \omega^2} \right)^{1/2} \quad (4.20)$$

and vertical wave number must be larger than a certain value of  $\eta_c$ .

In the atmosphere with positive temperature gradient less than  $2.2^\circ\text{C}/\text{km}$ , propagation of these frequency ranges are not permitted in vertical direction as well as in the case of isothermal atmosphere. Namely, no real value of vertical wave number  $\eta$  does exist.

Since  $H^2 > 0$ , sign of  $K^2$  is the same as  $\eta^2$ . Therefore, propagations permitted in y-x space are also permitted in z-x space. In other words, both these two coordinated systems are topologically equivalent.

It is interesting to note that when  $dT/dz = P_c$ . Then, writing  $\omega_A = \omega_B = \omega_0$  from Eq. (4.5), we get

$$\eta^2 = (\omega^2 - \omega_0^2) \cdot \left( \frac{1}{c^2} - \frac{k^2}{\omega^2} \right) \quad (4.16)$$

(i) if  $\omega > \omega_0$ ,  $\eta$  is real as far as  $k < \omega/c$ , and propagation surface is ellipsoid, corresponding to acoustic mode.

(ii) if  $\omega < \omega_0$ ,  $\eta$  is real only for  $k > \omega/c$  and propagation surface is hyperboloid limited in horizontal direction within asymptotic aperture

$$\theta_c = \text{tg}^{-1} \frac{\eta_c}{k_c} = \text{tg}^{-1} \sqrt{\frac{\omega_0^2 - \omega^2}{\omega^2}} \quad (4.17)$$

Therefore, at  $\omega = \omega_0$ ,  $\theta_c = 0$ , i.e., there is no vertical component of propagation vector for this frequency.

However, above discussion shows that if  $dT/dz > \Gamma_c$  no forbidden frequency exists in this layer of atmosphere. In this report, acoustic modes and gravity modes are continuous and can be called acoustic-gravity waves.

## 4.2 Dispersion

If  $dT/dZ < \Gamma_c$ ,  $\omega_B < \omega_A$  then dispersion relations are the same as before (3.2) and corresponding horizontal phase and group velocity are given by replacing  $\omega_b$  by  $\omega_B$ .

If  $dT/dZ > \Gamma_c$ , however,  $\omega_B > \omega_A$  and vertical phase and group velocities are given as follows:

(i)  $\omega > \omega_B > \omega_A$

From Eq. (4.5), phase velocity in vertical direction is

$$V_{ph} = \frac{\omega}{\eta} = \frac{\omega}{\sqrt{\omega^2 - \omega_A^2}} \cdot C \quad (4.18)$$

As  $\omega \rightarrow 0$ ,  $V_{ph} \rightarrow c$ , while  $\omega \rightarrow \omega_A$ ,  $V_{ph} \rightarrow \infty$ , but finite at  $\omega = \omega_B$

Group velocity in vertical direction is from Eq. (4.5)

$$V_g = \frac{d\omega}{d\eta} = \frac{\sqrt{\omega^2 - \omega_A^2}}{\omega} \cdot C \quad (4.19)$$

As  $\omega \rightarrow \infty$ ,  $V_g \rightarrow c$ , while  $\omega \rightarrow \omega_A$ ,  $V_g \rightarrow 0$ .

(ii)  $\omega_B > \omega > \omega_A$

$V_{ph}$  and  $V_g$  are the same as (4.18) and (4.19), respectively.

(iii)  $\omega_B > \omega_A > \omega$

No real value of  $\eta$  exists in the frequency range and wave propagation is limited in horizontal direction, corresponding thermobaric wave.

## 5. Normal Mode Calculation

As mentioned in the introduction, the previous calculation (M-W,1) shows that the pressure wave produced by periodical auroral heating attenuates quite rapidly outside the source. The fact that these traveling pressure waves are observed far outside the auroral zone during high geomagnetic activities, showing peculiar diurnal variation in their arrival direction (Chrzanowski et al 1961), indicates the importance of ducting for horizontal propagation of these waves in the atmosphere.

As shown in Fig. 4, there are two temperature minima in the earth's atmosphere, i.e., stratopause and mesopause, which are well known channels for sound wave propagation. Since sound velocity is minimum at the layer where temperature is minimum, ducting of sound waves are easily explained by ray-tracing by making use of Snell's law (or Fermat Principle).

In present problem, period of the wave is longer than 10 sec., and corresponding wave length is longer than 3 km. Therefore, the so-called Ray-theory is inapplicable but the ducting can be shown by the wave theory.

### 5.1 Multi-Isothermal-Layer Model

As discussed in the previous paper (M-W,1) and in section 3, the multiplication factors  $N(z)$  and  $M^2(z)$  in Eq. (2.8) are constant for the isothermal atmosphere, and solution is very simple as shown by Eq. (3.1), where two constant factors can be determined by two boundary conditions. Therefore, if we assume the atmosphere consisting of many isothermal layers, we can get a solution for this model atmosphere, connecting rigorous solutions at each layer by two boundary condition between each layer. If we assume  $n$ -layers, numbering from the bottom, these conditions are as follows;

- (i) At the ground, vertical velocity vanishes, i.e.,
- (ii) Between two layers, pressure variation and vertical velocity must be continuous, i.e.,

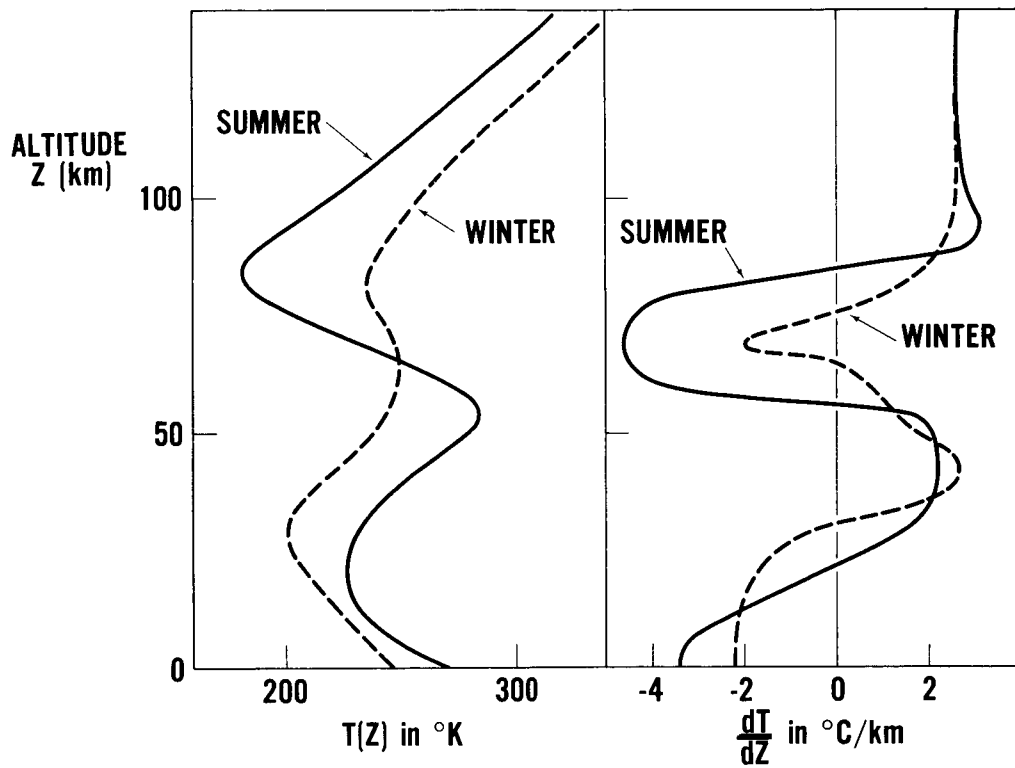


Figure 4—Vertical temperature distribution and lapse rate in the polar region for summer (full line) and for winter (dashed line).

$$p_n = p_{n-1} \quad \text{and} \quad W_n = W_{n-1}$$

$$p_1 = p_0 \quad W_1 = W_0 = W_{n=0}$$

(iii) at the top of atmosphere, kinetic energy (density) must be finite  
i.e.,  $\rho_n \cdot W_n^2 = \text{const.} \ (\text{const.} < \infty)$ .

Thus, we can determine  $2n$ -constants in the solutions of the type  
(3.1) for  $n$ -layers.

This technique has been developed by Pfiffer (1962) by making use  
of machine computer, and is applied for the interpretation of acoustic  
gravity wave propagation produced by A-bomb burst (Pfiffer and  
Zarichny, 1962, 1963).

Since the foundation of multi-isothermal layer approximation seems  
neither justified nor well established (Hines, 1964), only the following  
three-isothermal layer model is considered to see the ducting mechanism  
as follows:

The wave function (velocity divergence) in each layer can be  
written from Eq. (3.1) as,

$$\begin{aligned} \chi_1(z) &= C e^{n_1 z} + D e^{n_1^* z} & 0 \leq z \leq \\ \chi_2(z) &= A e^{n_2 z} + B e^{n_2^* z} & z_1 \leq z \leq z_2 \\ \chi_3(z) &= R e^{n_3 z} + e^{n_3^* z} & z_2 \leq z \leq \infty \end{aligned} \quad (5.1)$$

where

$$n_\ell = N_\ell + i \eta_\ell, \quad n_\ell^* = N_\ell - i \eta_\ell \quad (5.2)$$

$$N_\ell = \frac{\omega_A \ell}{C_\ell}, \quad C_\ell = \sqrt{\gamma R T_\ell} \quad (5.3)$$

$$\eta_\ell = \left[ \frac{\omega^2 - \omega_A^2 \ell}{C_\ell^2} - k^2 \left( 1 - \frac{\omega_B^2 \ell}{\omega^2} \right) \right]^{1/2} \quad (5.4)$$

$$\omega_A \ell = \frac{\gamma g}{2 C_\ell}, \quad \omega_B \ell = \frac{g}{C_\ell} \sqrt{\gamma - 1} \quad (5.5)$$

Suffix  $\ell$  indicates the number of layers from the bottom up, i.e.,  $\ell = 1, 2$  and  $3$ .

Incident wave at the top layer is assumed to be downward with a unit amplitude,  $e^{n_3^* z}$ .

Since propagation surface in the isothermal layer for acoustic mode ( $\omega > \omega_A > \omega_B$ ) is elliptic, as shown in Fig. 5, horizontal wave number  $k$  in the top layer gives the direction of wave propagation. The calculations are done for  $\tau = 100$  sec, taking  $\gamma$  as a parameter. Five constants appearing in Eq. (5.1) are uniquely determined by the following five boundary conditions, i.e.,

$$W_1(z = 0) = 0$$

$$W_1(z = z_1) = W_2(z = z_1), \quad p_1(z_1) = p_2(z_1) \quad (5.6)$$

and

$$W_2(z_2) = W_3(z_2), \quad p_2(z_2) = p_3(z_2)$$

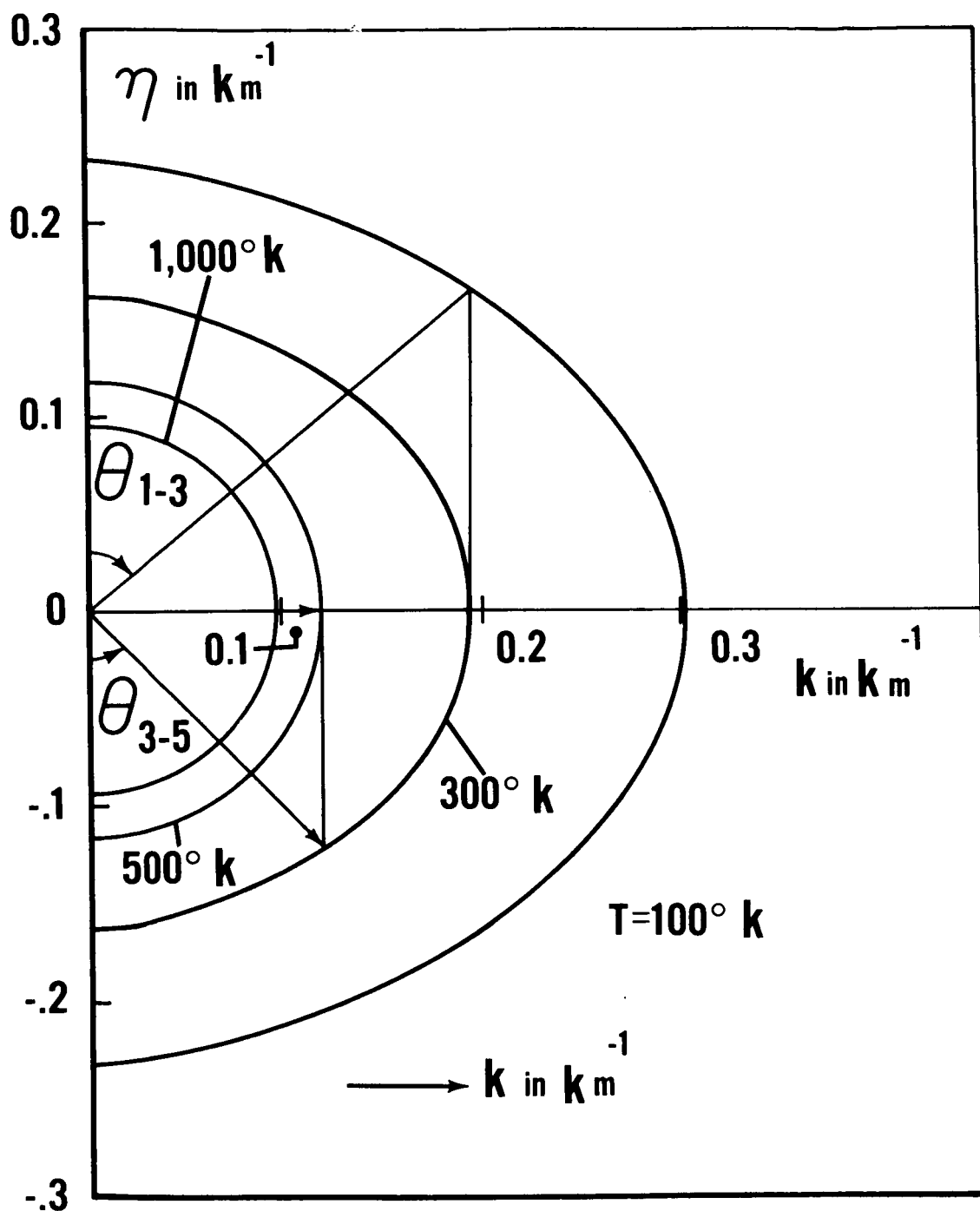


Figure 5—Cross-section of propagation surface in  $x$ - $z$  plane for the isothermal atmosphere in the different temperature.  $k$  and  $\eta$  stand for the wave number in horizontal ( $x$ -axis) direction and vertical ( $z$ -axis) direction, respectively.

where vertical velocity in each layer  $W_n(z)$  and pressure variation  $P_n(z)$  are given by

$$(g^2 k^2 - \omega^4) W_n(z) = \omega^2 C_n^2 \frac{d\chi_n}{dz} + g C_n^2 \left( k^2 - \frac{\gamma}{c_n^2} \omega^2 \right) \chi_n \quad (5.7)$$

and

$$P_n(z) = i \frac{\rho_0(z)}{\omega} (C_n^2 \chi_n - g W_n) \quad (5.8)$$

respectively.

Assuming  $z_1 = 50$  km and  $z_2 = 80$  km, amplitudes  $|A|$  and  $|C|$  are shown against  $k/k_c$  for two cases of temperature distributions in Fig. 6 and Fig. 7, in which temperature in each layer are also shown in the right hand side. Hatched domain indicates the wave of its energy is trapped in the middle layer, while other domains between curves  $|C|$  and  $|A|$  corresponds to the wave trapped in the bottom.

Fig. 7 shows that if the temperature of the middle layer is higher than those of other layers, no ducting occurs in the middle layer. However, as will be discussed later, other modes which correspond to internal gravity (thermobaric) wave has different mechanism for ducting.

This can be seen from Fig. 8, in which angular frequency of the traveling pressure wave  $\omega$  is plotted against horizontal wave number  $k$  (diagnostic diagram) for the isothermal atmospheres with a different temperature. Upper left part corresponds to acoustic mode while lower right part stands for internal gravity (thermobaric) mode. As shown by horizontal line (for example  $r = 100$  sec), acoustic waves propagating

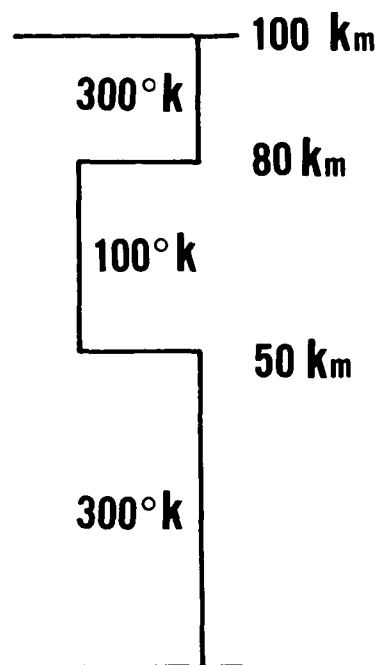
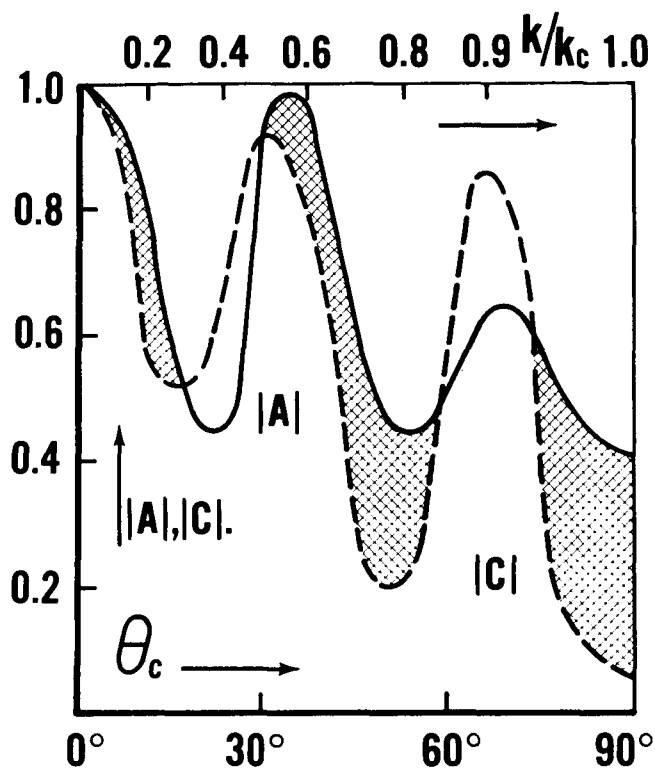


Figure 6—Amplitudes of upward propagating waves in the middle layer  $|A|$ , and in the bottom layer  $|C|$  for a model atmosphere (temperature distribution) shown in the right hand side. Full line and dashed line indicate  $|A|$  and  $|C|$ , respectively. The ratio of horizontal wave number in the top layer,  $k$ , to the critical value  $k_c$  is taken as horizontal axis, which corresponds also to the direction of propagation i.e.,  $k/k_c \approx \cos^{-1} \theta_c$  is a zenith angle of propagation direction.

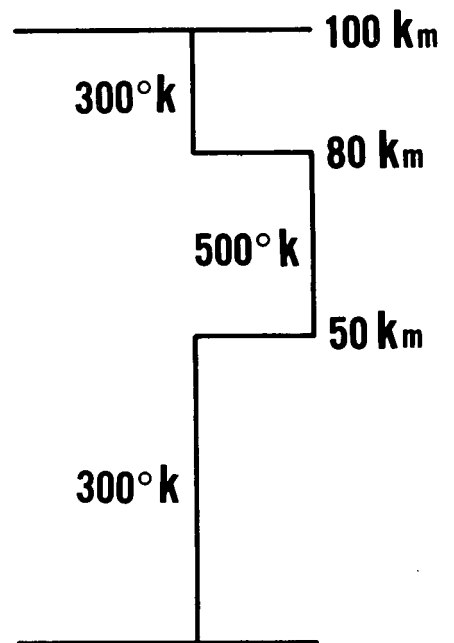
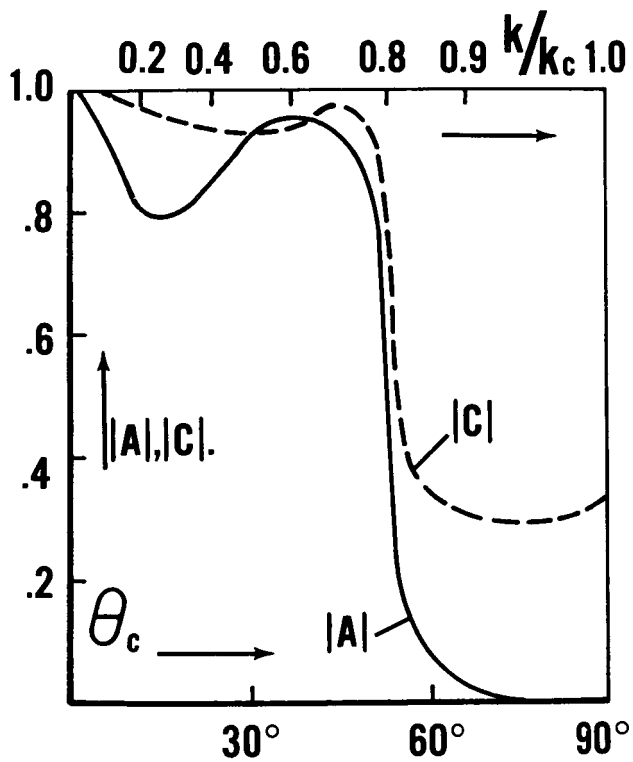


Figure 7—The same as Fig. 4 except different temperature in the middle layer as shown in the right hand side.

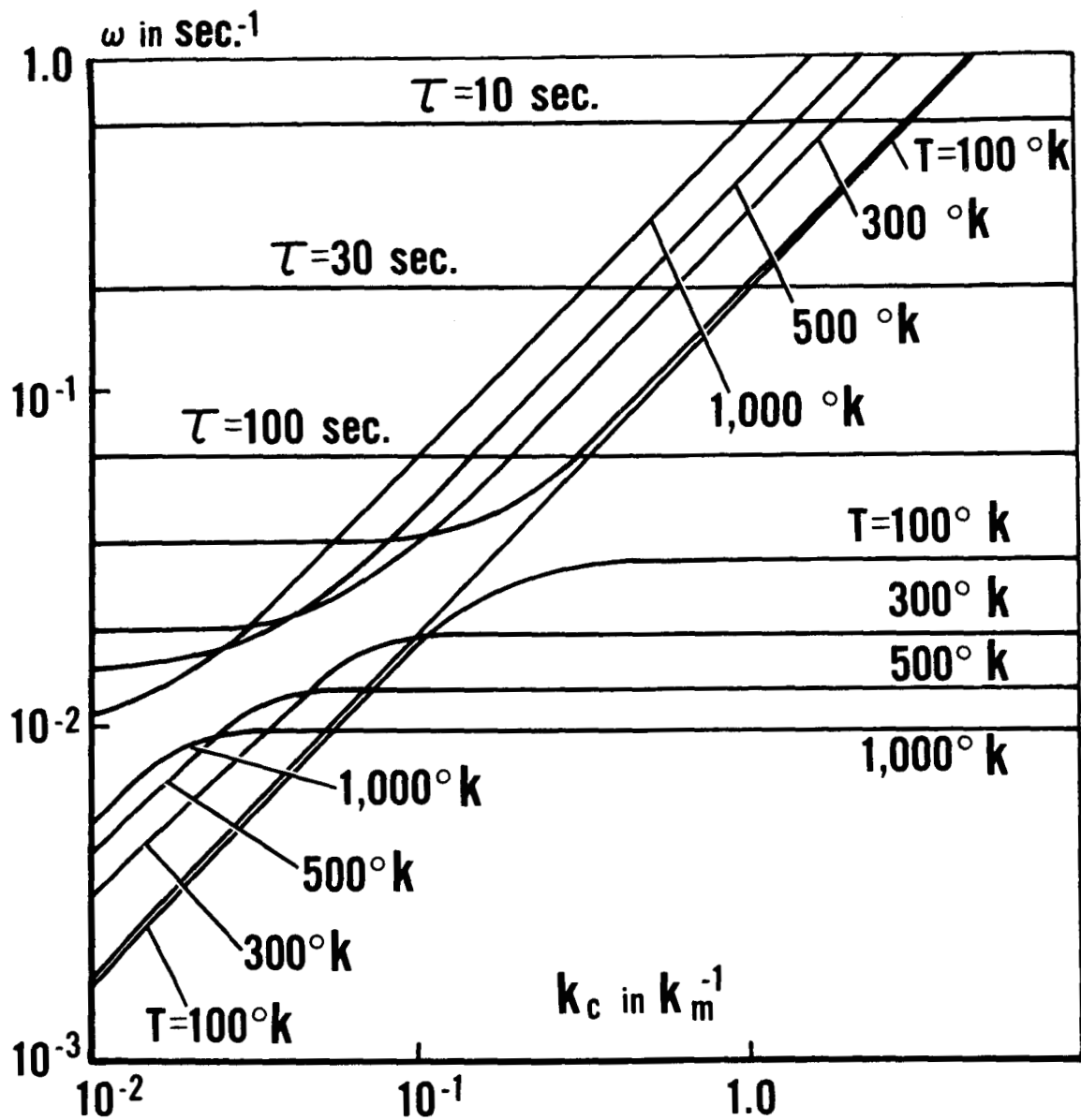


Figure 8—Diagnostic diagram for the isothermal atmospheres with different temperatures. Upper left and lower right domain corresponds to acoustic wave and internal gravity (or thermobaric) wave, respectively.

nearly horizontal direction, namely horizontal wave number  $k$  is very close to a critical value  $k_c$ , in a cold layer (for example  $T = 100^\circ\text{K}$ ) does not propagate into warmer layer (for example  $T = 300^\circ\text{K}$ ), of which critical wave number  $k_c$  is less than  $k$ . Since  $\eta_\ell$  becomes imaginary if  $k > k_c$  as can be seen from Eq. (5.4), the waves propagating in this layer with these wave numbers are not oscillatory any more but evanescent. However, the wavelength is quite long as compared with thickness of the layer (for example, for  $\tau = 100$  sec.,  $\lambda \simeq 30$  km), some fractions of wave energy can penetrate the barrier of warm layer, which is an exact analogy to "Tunnel effect" in quantum mechanics. By similar reason there is no forbidden direction in the propagation from warm layer to cold layer. Thus, as far as angular frequency is larger than  $\omega_A$  (i.e., period of the wave is shorter than  $\tau_A = 2\pi/\omega_A$ ), this mode of wave is trapped in the layer of minimum temperature.

If period  $\tau$  exceeds  $\tau_A$ , however, rather reverse situation occurs, which can be seen also from Fig. 8. Namely,

- (i) Since  $\tau_A$  is shorter in colder layer (see Eq. (5.5) or Eq. (3.3)), the wave of which period is very close to  $\tau_A$  in cold layer does not propagate into warmer layer in any direction and vice versa.
- (ii) If the period of the wave  $\tau$  exceed Brunt period  $\tau_B (= 2\pi/\omega_B)$ , any wave motion in coldest layer can propagate into warmer layer in any direction. In this respect, ducting for thermobaric mode is inverse of acoustic mode, and most of the kinetic energy of these long period

waves can be concentrated in the upper part (thermosphere) and lower part (near stratopause and bottom of troposphere), as shown by Pfiffer and Zarichny (1963).

## 5.2 W.K.B. - Approximation

As described in previous section 4, the wave equation in non-isothermal atmosphere (3.1) is written as (4.8), i.e.,

$$\frac{d^2 \phi(y)}{dy^2} + K^2(y) \phi(y) = 0 \quad (5.8)$$

where

$$K^2 = \eta^2 \cdot H^2(z) \quad (5.9)$$

if

$$\left| \frac{dK}{dy} / K^2 \right| \ll 1 \quad (5.10)$$

or

$$\left| \frac{dH}{dz} \right| \ll \eta \cdot H \quad (5.11)$$

solution of (5.8) can be given by the so-called W.K.B - approximation (for example, Budden 1961), that is

(i) for a range of  $y$ , where  $\eta^2 > 0$

$$\phi(y) \simeq C_1 K^{-1/2} \exp -i \int^y K(y') dy' + C_2 K^{-1/2} \exp i \int^y K(y') dy' \quad (5.12)$$

(ii) for a range of  $y$ , where  $\eta^2 < 0$

$$\phi(y) \simeq C_3 (K)^{-1/2} \exp - \int^y |K| dy \quad (5.13)$$

Those two types of solutions can be connected by making use of Airy function at the boundaries, where  $K(y) = 0$ . If the domains where

$\eta^2 > 0$  is limited by two solutions of  $K(y_1) = K(y_2) = 0$ , the normal mode condition is given from (5.12) as

$$\int_{y_1}^{y_2} K(y) dy = \left(n - \frac{1}{2}\right) \pi \quad (5.14)$$

where  $n$  is a positive integer.

Since  $dy = dz/H(z)$ , the left side of Eq. (5.14) is written as an integral by altitude  $z$ , i.e.,

$$\int_{z_1}^{z_2} \eta(z) dz = \left(n - \frac{1}{2}\right) \pi \quad (5.15)$$

In Fig. 9(a) and (b)  $K^2(z)$  is plotted against  $z$  for temperature distributions shown in Fig. 4 for  $\tau = 100$  sec. For acoustic mode, horizontal wave number is limited  $0 < k < k_c$ , corresponding horizontal wave length  $\lambda$  is  $\infty > \lambda > \lambda_c$ . Namely, there is a shortest wavelength  $\lambda_c$ , corresponding to horizontal propagation. Fig. 9 shows that horizontal propagation for  $\tau = 100$  sec wave is rather concentrated in mesosphere in summertime and in stratosphere in wintertime in polar region (Maeda, 1964).

Normal mode condition (5.15) is useful to find normal mode frequency or period if the criterion (5.10) or (5.11) is valid.

Since  $H(z) = \gamma RT(z)$ , inequality (5.11) is written also

$$\left| \frac{dT}{dz} \right| \ll \eta \cdot T(z) \quad (5.16)$$

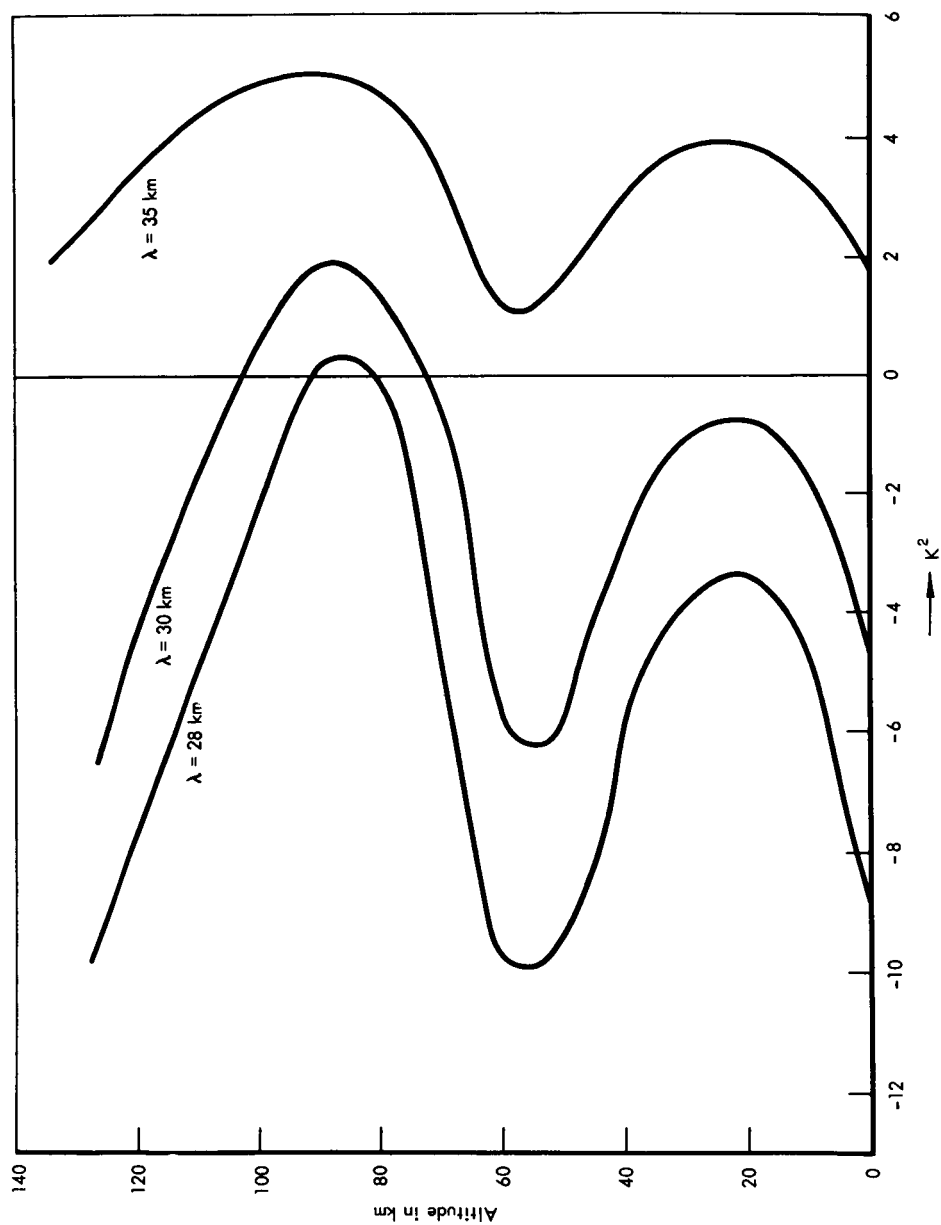


Figure 9(a)—Square of the index of refraction  $K^2$  for infrasonic waves with period 100 sec with summertime polar atmosphere, which temperature distribution is shown in Fig. 4 by full line.

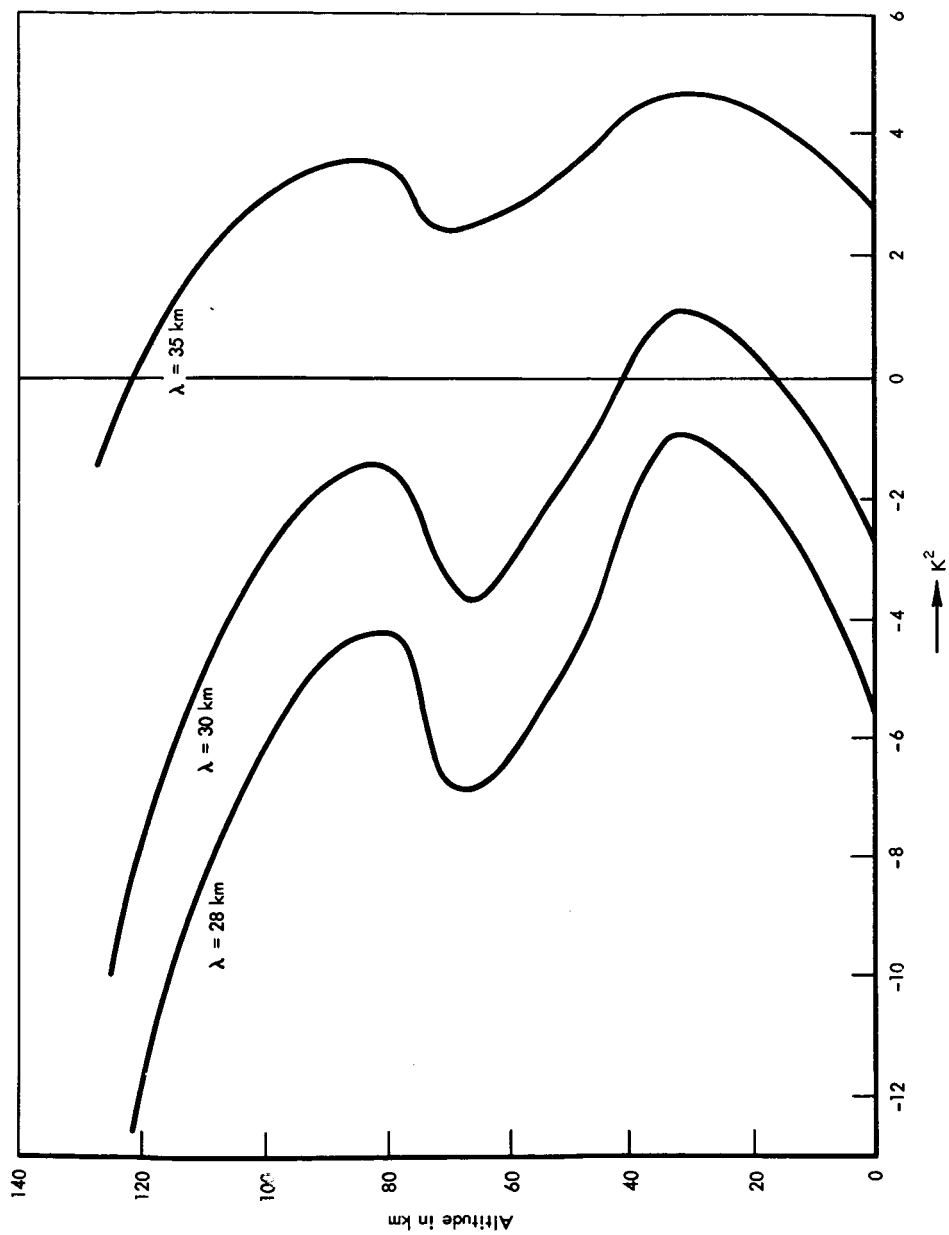


Figure 9(b)–The same as Fig. 9(a), except for wintertime polar atmosphere, which temperature distribution is shown in Fig. 4 by dashed line.

For  $\tau = 100$  sec.  $T(z) = 300^\circ\text{K}$ ,  $\eta \simeq 6 \cdot 10^{-2} \therefore \eta \cdot T \simeq 18$ . As shown in Fig. 4, at the lower part of thermosphere (around 90 km) and in mesosphere (around 60 km),  $|dT/dz| \simeq 5$ . Therefore, W.K.B. approximation for these long period waves is not good.

Thus, rigorous numerical integration is applied for the wave equation (2.8).

### 5.3 Direct Numerical Integration

Assuming incident downward wave at  $z = 100$  km, solution of Eq. (2.8) is computed numerically by means of Runge-Kutta method. Since boundary condition at the ground is  $W = 0$ , solution must satisfy the condition (from Eq. 5.7).

$$\frac{dX}{dz} - g \left( \frac{\gamma}{C^2} - \frac{k^2}{\omega^2} \right) h = 0 \text{ at } z = 0 \quad (5.17)$$

and for vertical propagation

$$\left. \frac{dX}{dz} \right|_{z=0} = g \frac{\gamma}{C^2} X(0) \quad (5.18)$$

In Fig. 10, some results of the wave period  $\tau = 100$  sec. are shown for a model of vertical temperature distributions shown in the left side. In the Figure I-A corresponds isothermal atmosphere, II-A stands for isothermal layer covered by warmer layer II above 80 km, while between 60 km and 80 km is a constant positive lapse rate layer, and I-B has a temperature minimum at 50 km.

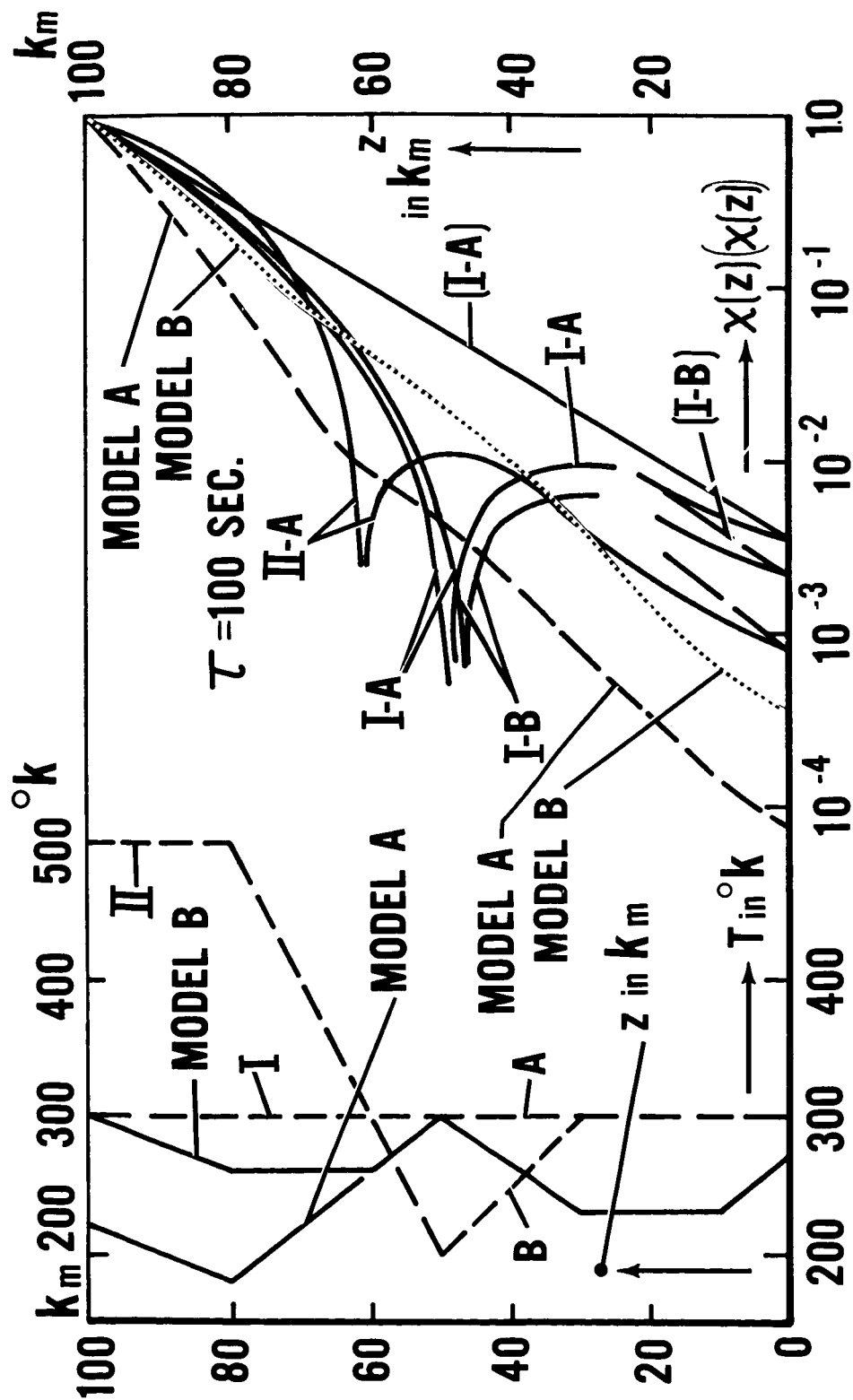


Figure 10—Results of numerical integration of wave equation with respect to a model atmosphere, of which vertical temperature distributions are shown in the left side. Explanation of the notation is given in text.

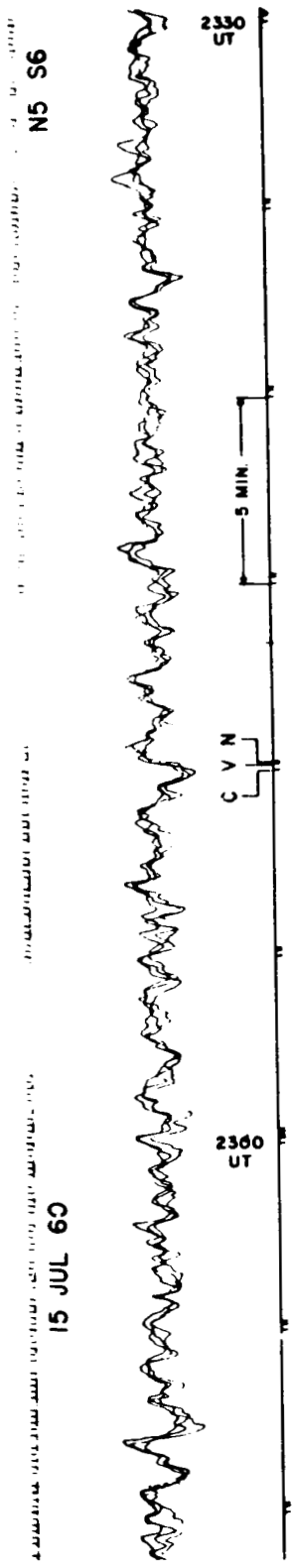
Results are shown only for the first mode. It is obvious that the amplitude of the wave, which satisfies the boundary condition at the ground, is largest in the isothermal atmosphere.

## 6. Data Analysis

Examples of traveling pressure waves during high geomagnetic activities recorded at the ground have been reported by Chrzanawski et al (1961) for observations at the NBS-station in Washington, D.C., and by Campbell and Young for the observation made at Alaska (inside of auroral zone).

As it is pointed out at the previous section (4.1 and 4.2), two modes of atmosphere internal pressure waves, i.e., acoustic and thermobasic mode, are continuous or overlapped at certain frequency ranges in the actual (non-isothermal) atmosphere. This can be seen from recorded data. For this purpose, we performed power spectrum analysis for the data, recorded at the NBS-stations in Washington, D.C., for a period between 21:00 and 24:00 UT on July 15, 1960. Superposed prints of these records in order to fix the arrival direction of the wave are shown in Fig. 11, and Kp-index around this period is shown in Fig. 12, in which the duration of the data shown in Fig. 11 is indicated by an arrow.

It should be noted the amplitude of these auroral pressure waves is of the order of one to ten dyne/cm<sup>2</sup>, while pressure waves produced by a large explosion (volcano, meteor and A-bomb) are of the order of several thousands dyne/cm<sup>2</sup> at a distance of several thousands km from



N3 S7

15 JUL 60



(1) > (2) < (3)

Figure 11—Superposed records of traveling pressure waves observed at the NBS-stations in Washington, D.C. C.V.N. correspond to data obtained at CARD, VILL and NAVE station shown in the paper by Chrzanowski et al (1961), respectively and the attached lines in the Figure shows the shifting of time between these records to fix the arrival direction.

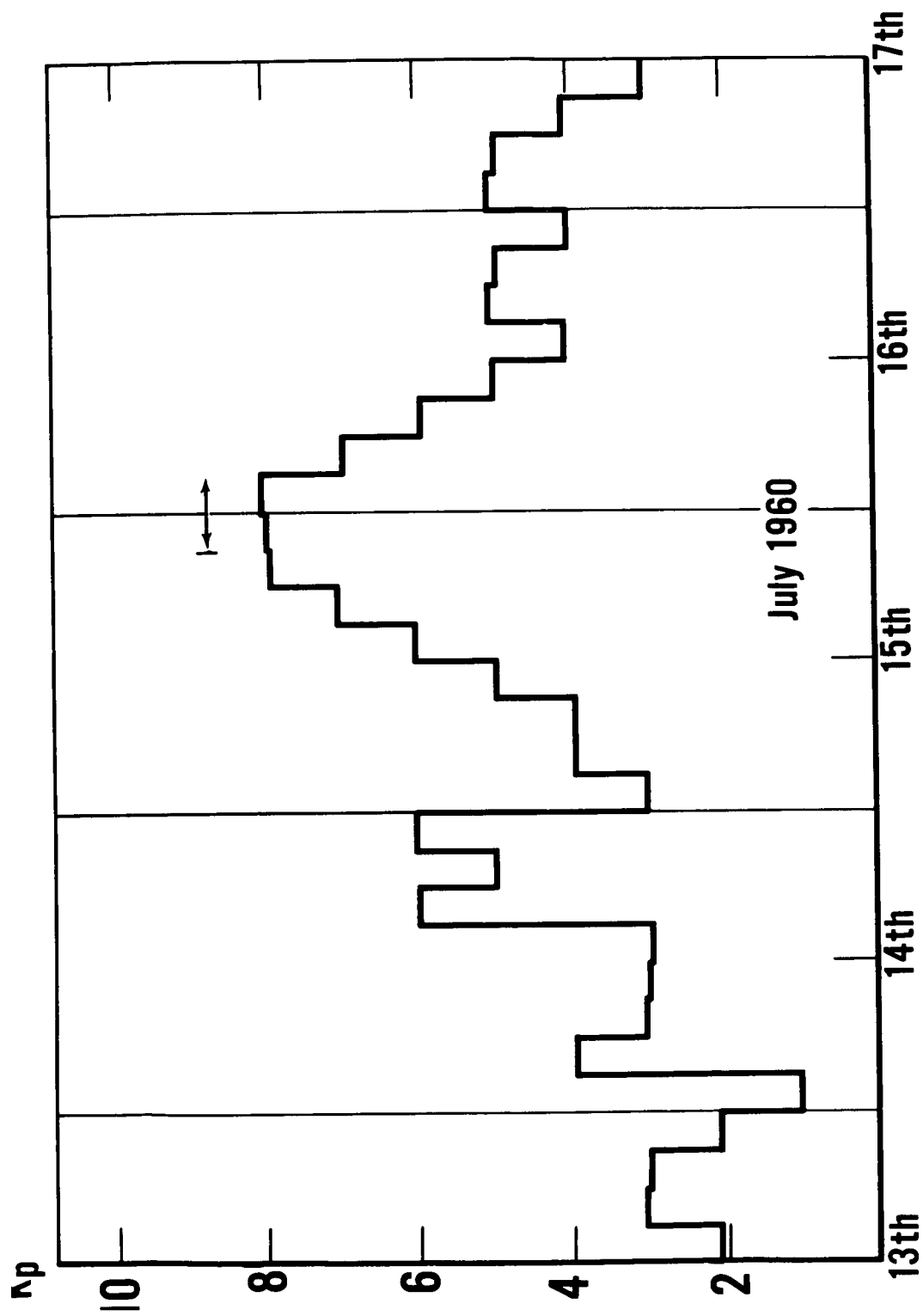


Figure 12-Kp-index during the period from July 13 to July 18, 1960. An arrow indicated the period, when power spectrum is applied for the records shown in Fig. 11.

the source. According to dispersion curves shown in Fig. 1, shorter waves appear first for acoustic mode and longer waves appear first for internal gravity waves.

### 6.1 Power Spectrum Analysis

Details of this method are well explained in a book written by Blackman and Tukey (1958) and have been applied many authors Panofsky and Liethbridge, 1958; Ness et al 1961, Ness, 1962, Stern 1962).

In present analysis, we applied the same method used by Pierson and Marks (1952) for analysis of ocean-wave records. Namely, non-normalized auto-correlation function  $Q_p$  is calculated by the formula

$$Q_p = \frac{2}{N-p} \sum_{n=1}^{N-p} P(t_n) P(t_{n-p}) \quad (p = 0, 1, 2 \dots m) \quad (6.1)$$

where  $P(t_n)$  and  $P(t_{n-p})$  are the readings of pressure wave record at time  $t_n$  and  $t_{n-p}$ .  $N$  is the total number of reading and  $m$  is the total number of shifting.

One example of  $Q_p$  is shown in Fig. 13, computed for a period indicated by number 1 in Fig. 11. Then raw-estimate of power spectrum is given by

$$L_h = \frac{1}{m} \left[ Q_0 + 2 \sum_{p=1}^{m-1} Q_p \cos \frac{\pi p h}{m} + Q_m \cos \pi h \quad (h = 0, 1, \dots m) \right] \quad (6.2)$$

where  $Q_p$  ( $p = 0, 1, \dots m$ ) is given by (6.1) and  $m$  is the total number of shifting.

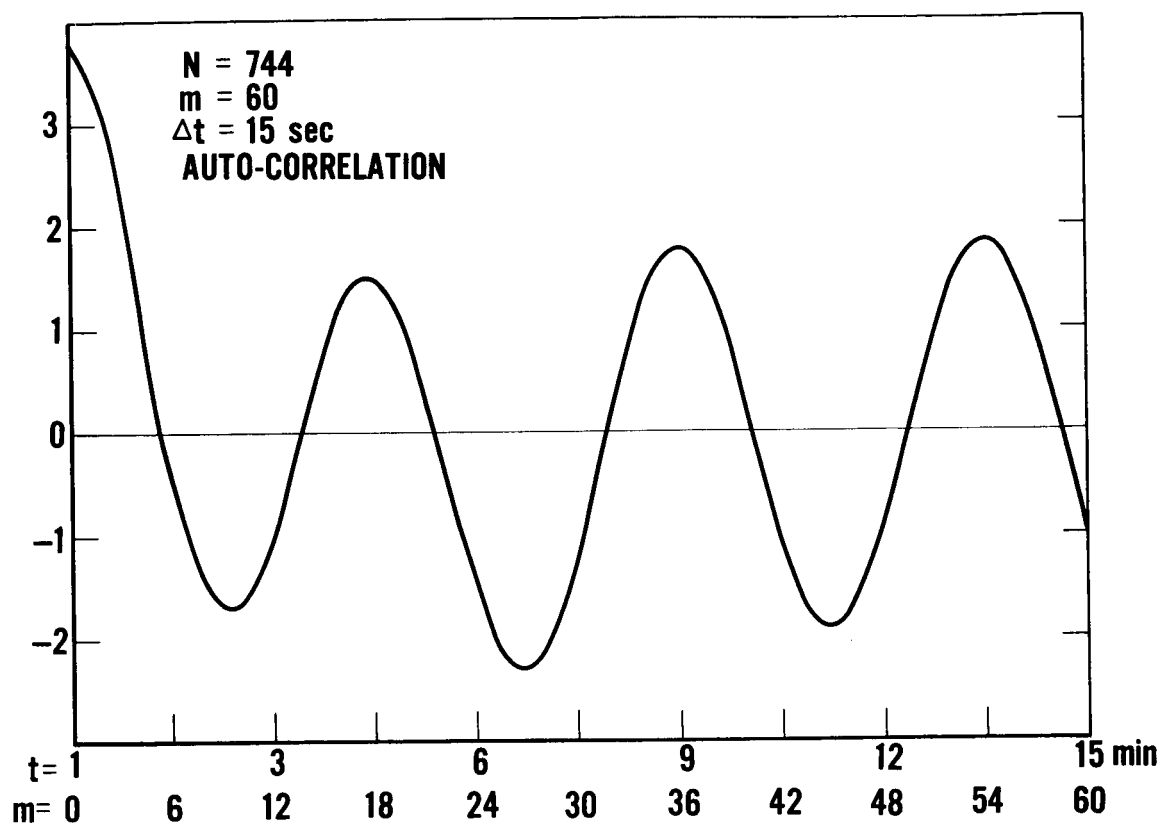


Figure 13—An example of non-normalized auto-correlation curve for period shown in Fig. 11. The total number of reading  $N$ , and number of shifting  $m$ , are 744 and 60, respectively, while digitized reading interval  $\Delta t$  is 15 sec.

It is assumed for these analyses that recorded pressure variations are quasi-stationary and that the period of the wave is far shorter than the length of the period used for analysis. Strictly speaking, none of these is satisfied and there is an error due to the difference between this assumption and real situation, particularly discrete reading by digitization and a finite length of the data. This error can be, however, reduced by making use of a filter. One of the simplest filters used present computation, and the result is given by

$$L_h = 0.23 L_{h-1} + 0.54 L_h + 0.23 L_{h+1} \quad (6.3)$$

$$(h = 0, 1, \dots m)$$

Namely, this is essentially the same running weight average.  $L_h$  and  $U_h$  are shown in Fig. 14, corresponding to auto-correlation function shown in Fig. 13.

Similar results corresponding to the period indicated by number 2 and 3 are also shown in Fig. 15 and 16, respectively, where full line and dashed line correspond to  $U_h$  and  $L_h$  respectively. Since sensitivity of the recorder is not uniform, corrected value for the sensitivity of the recorder is also shown in Fig. 16 by a curved  $U_{hc}$ .  $U_h$  in Fig. 16 is replotted against period (in sec.) in Fig. 17, which shows the most dominating period of the wave in this stage of wave appearance is around 50 sec and has a long tail towards longer period. Sharp cut-off in short period around 10 sec might be, however, interpreted as due to a limitation in digitization of the data.

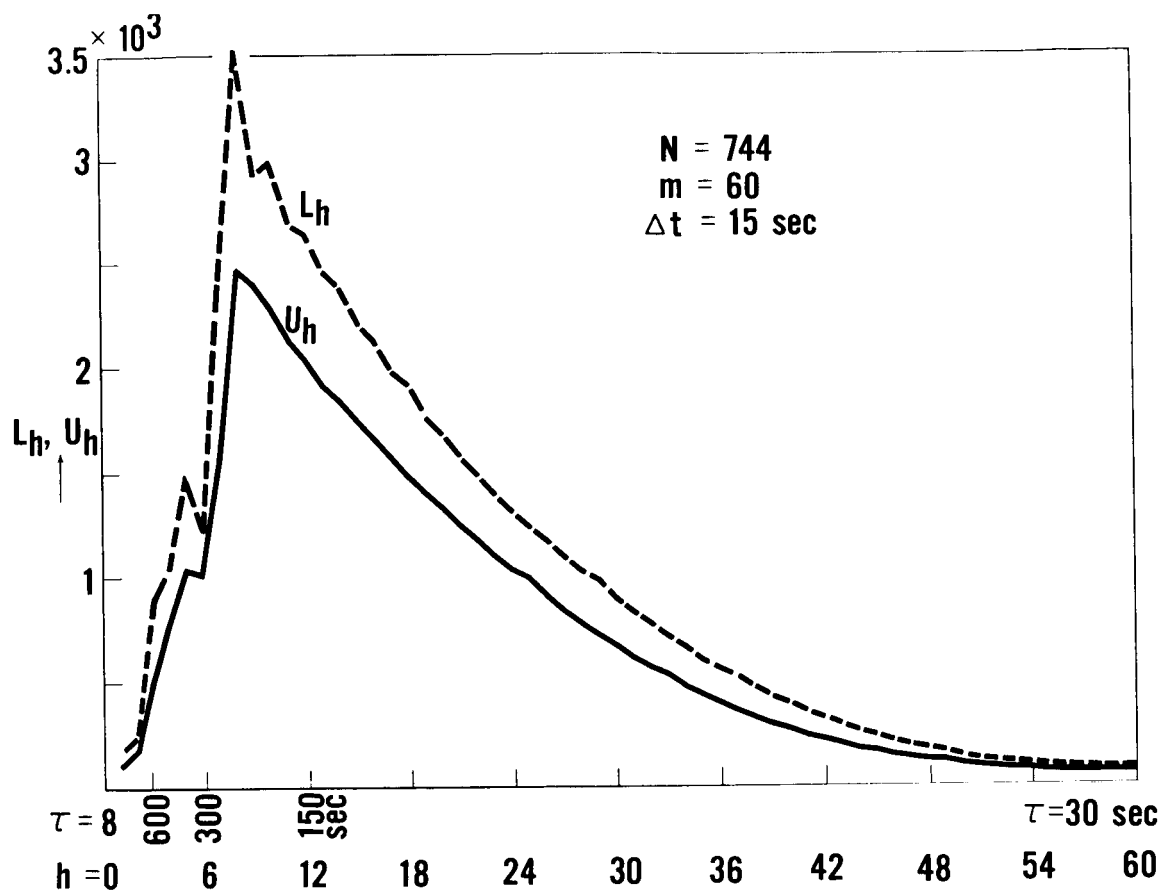


Figure 14—Power spectrum corresponding to the data used for Fig. 13, where  $L_h$  is raw estimate (without filter) and  $U_h$  is smoothed value eliminating noise.

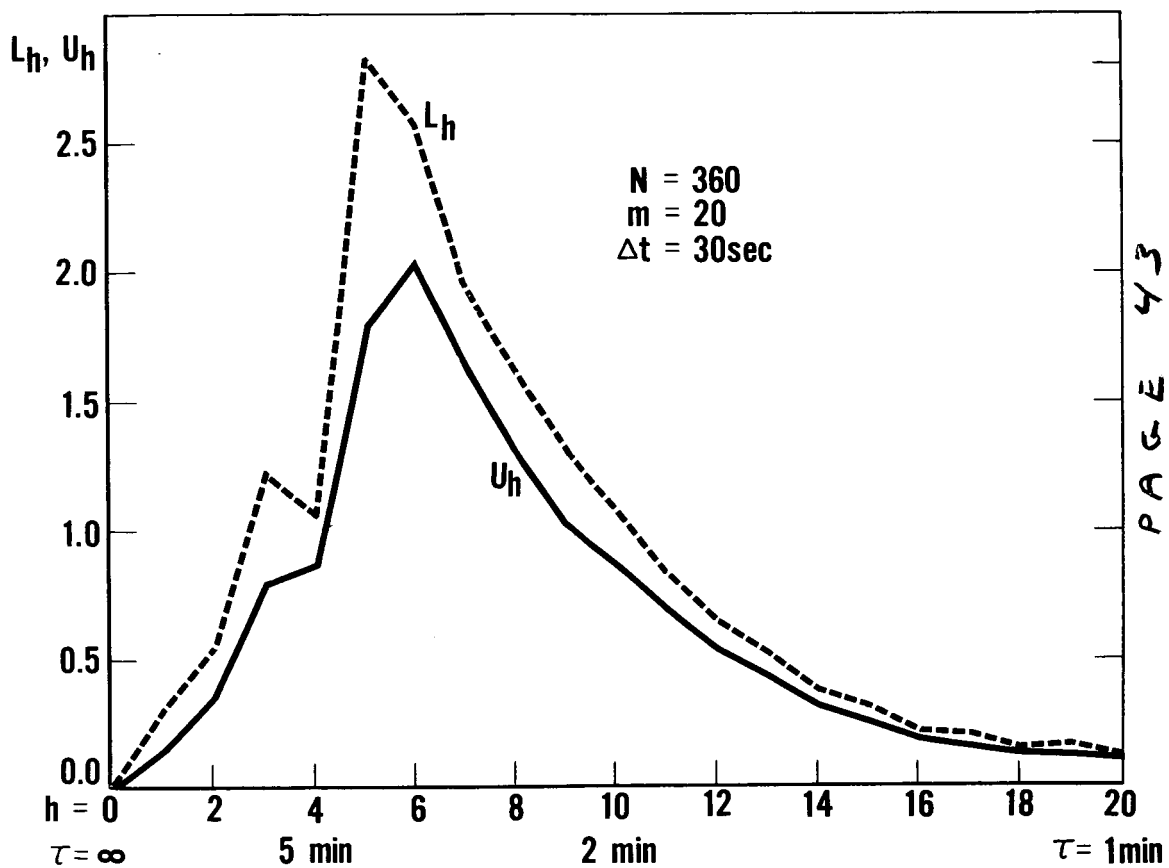


Figure 15—Power spectrum for the period indicated by number 2 in Fig. 11.

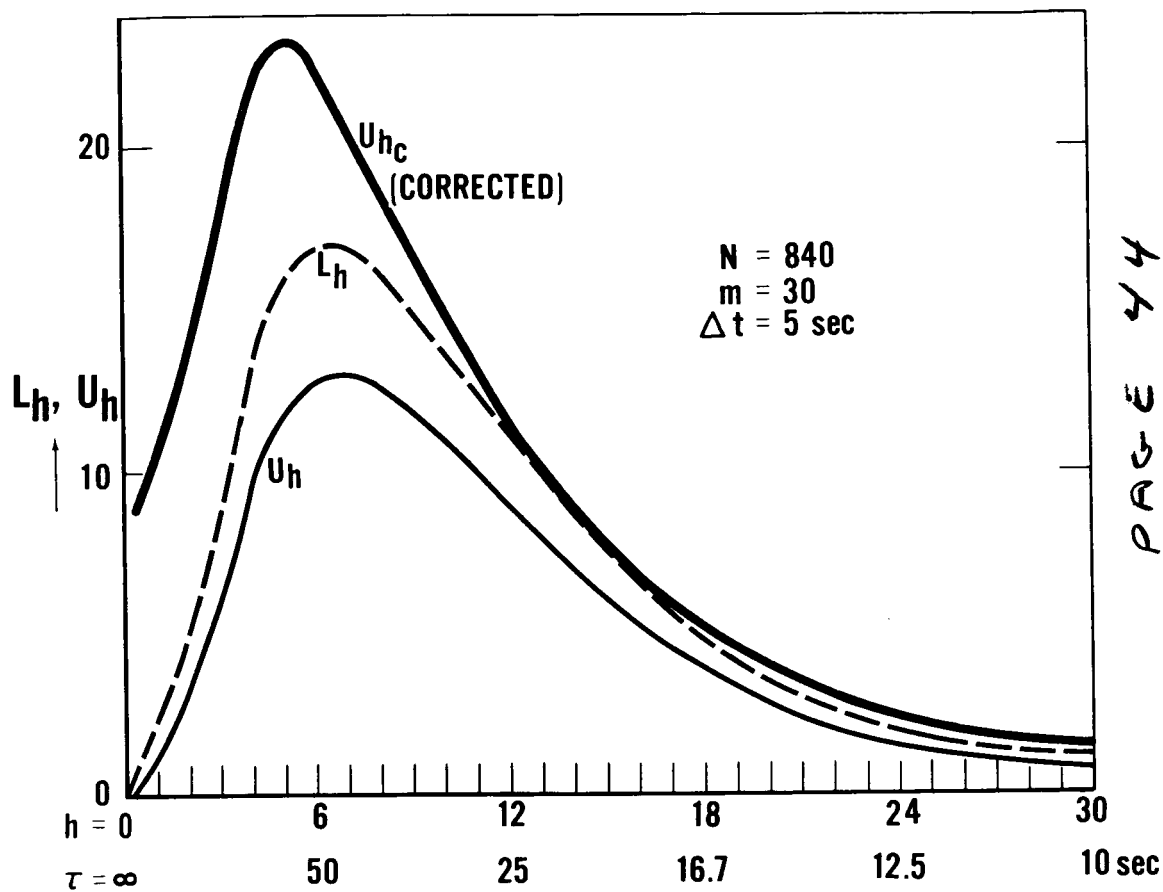


Figure 16—The same as Fig. 14 and 15, for the period of last phase, shown by number 3 in Fig. 11.

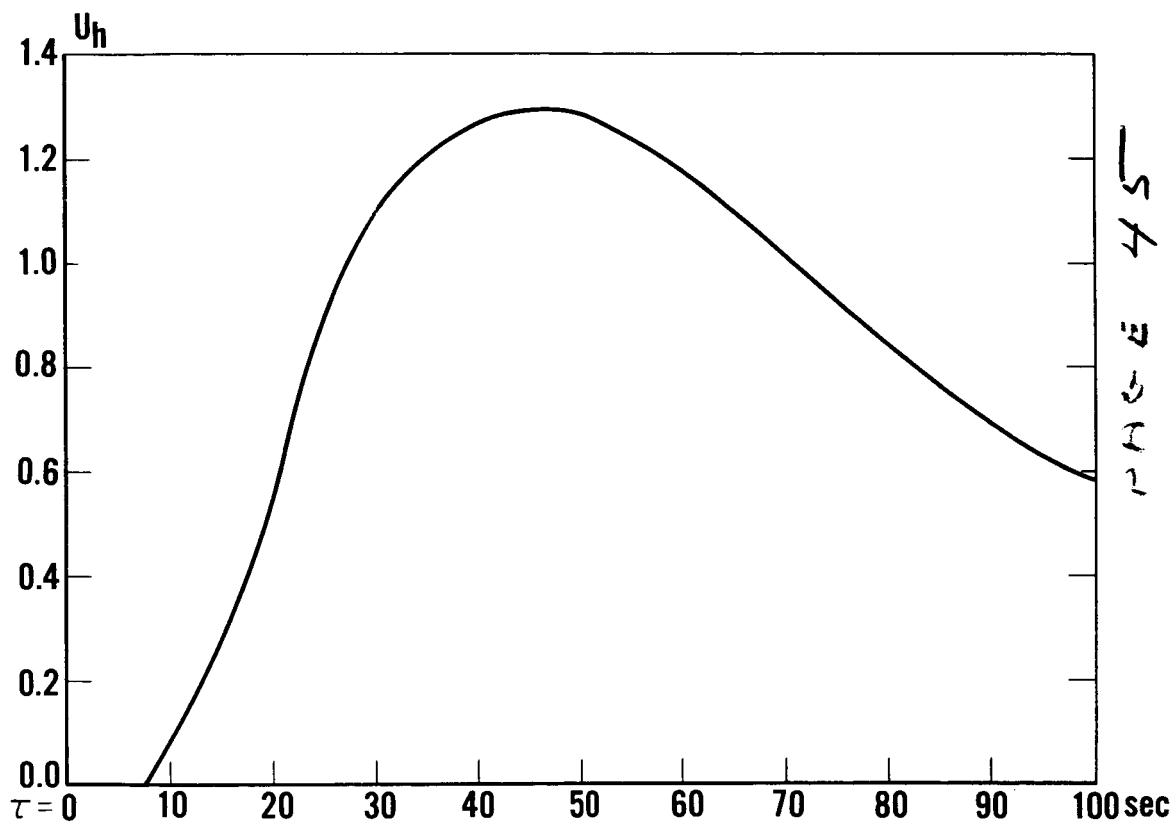


Figure 17—Wave spectrum of  $U_h$  in Fig. 16 plotted against  $\tau$  in sec.

## 6.2 Wave Form and Airy Phase

As can be seen from Fig. 11, during a period extending from around 21:20 UT to 22:30 UT, pressure wave shows a clear sinusoidal oscillation, while before and after this period the waveforms are smeared by superposed short waves. As shown in Fig. 1, dependence of group velocity on the period of pressure wave in the isothermal atmosphere is opposite each other between acoustic mode and thermobaric mode, leaving a minimum around 300 sec for 300°K atmosphere, where the group velocity of both waves is zero.

According to Pfeffer and Zarichny (1963), several minima appear around this period in the actual atmosphere, corresponding to different normal mode propagations. It is clear, however, that even in the non-isothermal atmosphere at a certain distant point from the source, the acoustic mode of pressure wave should be observed short wave first and longer wave later, while thermobaric mode of wave arrives long wave first and shorter one follows in the last. Although the effective height of propagation is different by wave-period (Pfeffer and Zarichny, 1963), it is possible that at a certain point from the source two types of wave overlap with same period (i.e., the same horizontal wave length) for a certain duration, which corresponds to minima of group velocities. As discussed in previous section (section 4.1 and 4.2), in the non-isothermal atmosphere, there are domains where both mode of atmospheric wave continues. Therefore, an occasional appearance of clear sinusoidal oscillation of pressure wave during auroral activities can be

ascribed to this mechanism, which is quite similar to the so-called Airy Phase effect observed in a sound wave propagation under shallow water (Pekeris, 1948).

## 7. Discussion

As pointed out in the introduction, the amplitude of pressure wave associated with auroral activity observed at the ground is of the order of one to ten dynes/cm<sup>2</sup> and dominating period is within the acoustic mode, i.e., mostly between 40 to 80 sec. On the other hand, the amplitudes of blast wave produced by volcanic, large meteorite and bomb explosion are order of several hundred to thousand dynes/cm<sup>2</sup> (i.e., 0.3 to 3 mb) at the ground more than 1,000 km from the source, and period of the wave is in gravity mode (more than 5 min). Another difference between these types of atmospheric waves is seen in trend of wave form. Namely, most of auroral pressure wave appears with shorter wave first (Chrzanowski et al 1961), while pressure waves detected by microbarograph after large explosion show the arrival of longer wave first and the shorter wave later (Hunt et al 1960).

These are exactly what we can expect from dispersion relations for both modes of atmospheric pressure wave (Fig. 1). However, as shown in present paper, auroral activity can produce both types of atmospheric waves. Moreover, in this case, we see the so-called Airy phase effect, which is known in a sound propagation in shallow water (Pekeris, 1948).

One of the important problems, which is omitted in this paper is the mechanism of wave-generation. This is briefly discussed in previous paper (M-W,1), and we concluded that one of the most effective and plausible mechanisms is periodic heating of E-region by impinging auroral electrons. In the isothermal atmosphere at least  $100 \text{ erg/cm}^2 \text{ sec}$  of energy flux is required to produce the infrasonic waves with amplitude  $1 \text{ dyne/cm}^2$  at the ground. In the isothermal atmosphere, however, these thermally excited atmospheric waves attenuate rapidly outside the source region particularly at short periods. In the actual atmosphere, there are two channels for ducting corresponding to two temperature minima at the tropopause and the mesopause (Fig. 4).

The minimum energy flux required to produce observable pressure waves at the ground is therefore one or two order of magnitude higher than the one estimated for the isothermal atmosphere as can be seen from Fig. 12 and 14.

It is also shown that effective duct for 100 sec pressure wave in the polar atmosphere is the upper channel in summer and the lower one in winter (Fig. 9 a and b).

## References

1. Chrzanowski, P., G. Greene, K. T. Lemmon and J. M. Young.,  
"Travelling Pressure Waves Associated with Geomagnetic Activity,"  
J. Geophys. Res. 66, 3727-3733, 1961
2. Maeda, K, and T. Watanabe, "Pulsating Aurorae and Infrasonic  
Waves in the Polar Atmosphere," J. Atmos. Sci. 21, 15-29, 1964a
3. Maeda, K., and T. Watanabe, "Infrasonic Waves from the Auroral  
Zone," NASA TN D-2138, June 1964b
4. Campbell, W. H., and J. M. Young, "Auroral-Zone Observations of  
Infrasonic Pressure Waves Related to Ionospheric Disturbances and  
Geomagnetic Activity," J. Geophys. Res. 68, 5909-5916, 1963
5. Eckart, C., "Hydrodynamics of Oceans and Atmosphere," Pergamon  
Press, 1960
6. Tolstoy, I., "The Theory of Waves in Stratified Fluids Including the  
Effects of Gravity and Rotation," Rev. Mod. Phys. 35, 207-230, 1963
7. Obayashi, T., "Upper Atmosphere Disturbances Due to High Altitude  
Nuclear Explosions," Planet. Space. Sci. 10, 47-63, 1963
8. (8.1) Hines, C.O., Integral Atmospheric Gravity Waves at Ionosphere  
Heights," Can. J. Phys. 38, 1441-1481, 1960  
  
(8.2) Atmospheric Gravity Waves: A New Toy for the Wave Theorist,"  
Reprint, to be published in Radio Science. 1964b  
  
(8.3) A private communication, 1964a
9. Martyn, D.F., "Cellular Atmospheric Waves in the Ionosphere and  
Troposphere," Proc. Roy. Soc. Lond. 201A, 216-233, 1950
10. Yamamoto, R., "A Study of the Microbarographic Waves," Jour.  
Met. Soc. Japan, 34, 235-243, 1956

11. Gossard: Vertical Flux of Energy into the Lower Ionosphere from Internal Gravity Waves Generated in the Troposphere," T.G.R. 67, 745-757, 1962
12. Pekeris, C. L., "The Propagation of a Pulse in the Atmosphere, Part II," Phys. Rev. 73, 145-154, 1948
13. Lamb, H., "Hydrodynamics," N.Y. Dover, 1932
14. Pfeffer, R. L., "A Multi-layer Model for the Study of Acoustic-Gravity Wave Propagation in the Earth's Atmosphere," J. Atm. Sci. 19, 251-255, 1962
15. Pfeffer, R. L., and J. Zarichny, "Acoustic-Gravity Wave Propagation from Nuclear Explosions in the Earth's Atmosphere," J. Atm. Sci. 19, 256-263, 1962  
  
Pfeffer, R. L., "Acoustic-Gravity Wave Propagation in an Atmosphere with Two Sound Channels," Geofisica Pura e Applicata, 55, 175-199, 1963
16. Hunt, J. N., R. Palmer and W. Penney; "Atmospheric Waves caused by Large Explosions," Phil. Trans. Roy. Soc. 252A, 275-315, 1960
17. Budden, K. G., "Radio Waves in the Ionosphere," Cambridge University Press. 1961
18. Maeda, Kaichi, "On the Acoustic Heating of the Polar Night Mesosphere," T.G.R. 69, 1381-1395, 1964
19. Blackman, R. B., and J. W. Tuckey, "The Measurement of Power Spectra," Dover Publications, Inc. N. Y. 1958
20. Ness, N.F., J. C. Harrison and L. B. Slichter, "Observation of Free Oscillations of the Earth," T.G.R. 66, 621-629, 1961

21. Stern, D., "The Low-Frequency Power Spectrum of Cosmic Ray Variations during IGY," T.G.R. 67, 2133-2144, 1962
22. Pierson, W. J., and W. Mark, "The Power Spectrum Analysis of Ocean Wave Records," Trans. Amer. Geophys. Union 33, 834-844, 1952
23. Pekeris, C. L., "Theory of Propagation of Explosive Sound in Shallow Water," Geological Soc. Amer. Memo. 27, 1-117, 1948

## Captions

Fig. 1. Horizontal wave velocities in the isothermal atmosphere ( $T = 300^\circ\text{K}$  and  $C = 0.347 \text{ km/sec}$ ) against period of the wave  $\tau$  (in.sec) full lines and dashed lines are phase velocities and group velocities, respectively.

Fig. 2. Hines' angular frequency  $\omega_A$  and Brunt-Varsola angular frequency  $\omega_B$  as a function of altitude  $z$ , for the vertical temperature distribution  $T(z)$  shown by full line in Fig. 4.

Fig. 3. The same as Fig. 2 for the vertical temperature distribution shown in Fig. 4 by dashed line.

Fig. 4. Vertical temperature distribution and lapse rate in the polar region for summer (full line) and for winter (dashed line).

Fig. 5. Cross-section of propagation surface in  $x$ - $z$  plane for the isothermal atmosphere in the different temperature.  $k$  and  $\eta$  stand for the wave number in horizontal ( $x$ -axis) direction and vertical ( $z$ -axis) direction, respectively.

Fig. 6. Amplitudes of upward propagating waves in the middle layer  $|A|$ , and in the bottom layer  $|C|$  for a model atmosphere (temperature distribution) shown in the right hand side. Full line and dashed line indicate  $|A|$  and  $|C|$ , respectively. The ratio of horizontal wave number in the top layer,  $k$ , to the critical value  $k_c$  is taken as horizontal axis, which corresponds also to the direction of propagation i.e.,  $k/k_c \simeq \cos^{-1} \theta_c$ , where  $\theta_c$  is a zenith angle of propagation direction.

Fig. 7. The same as Fig. 6 except different temperature in the middle layer as shown in the right hand side.

Fig. 8. Diagnostic diagram for the isothermal atmospheres with different temperatures. Upper left and lower right domain corresponds to acoustic wave and internal gravity (or thermobaric) wave, respectively.

Fig. 9 (a). Square of the index of refraction  $K^2$  for infrasonic waves with period 100 sec with summertime polar atmosphere, which temperature distribution is shown in Fig. 4 by full line.

Fig. 9 (b). The same as Fig. 9 (a), except for wintertime polar atmosphere, which temperature distribution is shown in Fig. 4 by dashed line.

Fig. 10. Results of numerical integration of wave equation with respect to a model atmosphere, of which vertical temperature distributions are shown in the left side. Explanation of the notation is given in text.

Fig. 11. Superposed records of traveling pressure waves observed at the NBS-stations in Washington, D.C. C.V.N. correspond to data obtained at CARD, VILL and NAVE station shown in the paper by Chrzanowski et al (1961), respectively and the attached lines in the Figure shows the shifting of time between these records to fix the arrival direction.

Fig. 12. Kp-index during the period from July 13 to July 18, 1960. An arrow indicated the period, when power spectrum is applied for the records shown in Fig. 11.

Fig. 13. An example of non-normalized auto-correlation curve for period shown in Fig. 11. The total number of reading  $N$ , and number of shifting  $m$ , are 744 and 60, respectively, while digitized reading interval  $\Delta t$  is 15 sec.

Fig. 14. Power spectrum corresponding to the data used for Fig. 13, where  $L_h$  is raw estimate (without filter) and  $U_h$  is smoothed value eliminating noises.

Fig. 15. Power spectrum for the period indicated by number 2 in Fig. 11.

Fig. 16. The same as Fig. 14 and 15, for the period of last phase, shown by number 3 in Fig. 11.

Fig. 17. Wave spectrum of  $U_h$  in Fig. 16 plotted against period  $\tau$  in sec.